Mechanical Systems and Signal Processing

On the Investigation of Ash Deposition Effect on Flow-Induced Vibration Energy Harvesting

--Manuscript Draft--

Manuscript Number:	MSSP21-3265R2
Article Type:	Standard Research Article
Keywords:	ash deposition; energy harvesting; flow-induced vibration; galloping; vortex-induced vibration
Corresponding Author:	Guobiao Hu, Ph.D. Nanyang Technological University SINGAPORE
First Author:	Junlei Wang, PhD
Order of Authors:	Junlei Wang, PhD
	Shanghao Gu, PhD
	Daniil Yurchenko, PhD
	Guobiao Hu, Ph.D.
	Ronghan Wei, PhD
Abstract:	This paper proposes harnessing the aerokinetic energy in flue systems and it explores the effect of the ash deposition on flow-induced vibration energy harvesting performance. Bell-shaped and horn-like bluff bodies are designed to simulate different ash depositions on a conventional elliptic cylinder bluff body. Wind tunnel experiments were conducted to investigate the energy harvesting performance using different ash deposition distributed over the bluff bodies. The experimental results show that compared to the baseline model of a conventional elliptic cylinder bluff body, the bell-shaped bluff body suppresses the flow-induced vibration and deteriorates the energy harvesting performance. In contrast, the horn-like bluff body can benefit energy harvesting by reducing the galloping cut-in wind speed and increasing the voltage output. The voltage output of an optimal prototype using the horn-like bluff body is increased by 516%. Computational fluid dynamics (CFD) simulations were carried out to unveil the physical mechanisms behind the phenomena. The CFD analysis results indicate that the appearance of the small-scale secondary vortices (SV) widens the wake flow and increases the aerodynamic force produced by the horn-like bluff body. The flow-induced vibration of the harvester using the horn-like bluff body transforms from VIV to galloping. Therefore, it has been preliminarily demonstrated that the unfavorable ash deposition phenomenon in flue systems has the potential for promoting flow-induced vibration energy harvesting.

Powered by Editorial Manager® and ProduXion Manager® from Aries Systems Corporation

Dear Editors of Mechanical Systems and Signal Processing:

We would like to submit our manuscript entitled "***On the Investigation of Ash Deposition Effect on Flow-Induced Vibration Energy Harvesting***" for possible publication in Mechanical Systems and Signal Processing. We declare that there is no conflict of interest between the authors, and this is an original work that has not been published previously and is not under consideration for publication elsewhere, in whole or in part.

This paper proposes to install a flow-induced piezoelectric energy harvester (FIVPEH) in flues or heat exchange systems where aerokinetic energy exists. Ash deposition is an inevitable phenomenon during the combustion process. Therefore, the ash deposition on the elliptic cylinder bluff body is considered, and its effect on the energy harvesting performance is investigated. According to the ash deposition types summarized in the literature, bell-shaped and horn-shaped cylinder bluff bodies are designed to consider the ash deposition effect on a conventional elliptic cylinder bluff body. Wind tunnel experiments are conducted to investigate the energy harvesting performance using different ash deposition attached bluff bodies. It has been found that though the ash deposition of dusty flue gas in the boiler and heat exchanger often threatens the safety of the equipment and affects the heat exchange performance, horn-like ash deposition formed on the elliptic cylinder bluff body can benefit energy harvesting by reducing the cut-in wind speed and increasing the voltage output. Computational fluid dynamics (CFD) simulations are carried out to explain the physical mechanisms behind the phenomena.

We deeply appreciate your consideration of our manuscript and look forward to receiving comments from the reviewers. If you have any queries, please don't hesitate to contact us.

Thank you and best regards.

Yours sincerely,

Corresponding author: Dr. Guobiao Hu

E-mail: guobiao.hu@ntu.edu.sg

Responses to review comments

We are thankful for the time and efforts of the editor and reviewers. The review comments are valuable for us to improve the quality of our manuscript. We have considered and addressed all the comments from the reviewers, and the detailed point-to-point response is given below in red. The changes in the revised manuscript are highlighted in yellow.

Reviewer #1:

The authors have responded adequately to my concerns on the original submission, and they have made appropriate revisions to the paper. I therefore recommend acceptance of the paper for publication in MSSP.

While reading the paper, I have made a number of linguistic corrections and improvements, which may be found in the attached marked typescript, for the authors to consider/implement.

Response: Thanks to the reviewer for recommending our paper. We sincerely appreciate that the reviewer has made a number of linguistic corrections and improvements. We have made corresponding modifications in the revised manuscript by following the typescript from the reviewer.

REVISED Manuscript (Clean version in Editable Format)

Click here to view linked References

On the Investigation of Ash Deposition Effect on Flow-Induced Vibration Energy Harvesting

Junlei Wang[1], Shanghao Gu[1], Daniil Yurchenko[2], Guobiao Hu[3,4*], Ronghan Wei[5,6]

[1] School of Mechanical and Power Engineering, Zhengzhou University, Zhengzhou 450000, China

[2] Institute of Sound and Vibration Research, University of Southampton, Southampton, SO17 1BJ, UK.

[3] School of Civil and Environmental Engineering, Nanyang Technological University, 50 Nanyang Avenue, 639798, Singapore

[4] State Key Laboratory of Structural Analysis for Industrial Equipment, Dalian University of Technology, Dalian 116024, China

[5] School of Mechanics and Safety Engineering, Zhengzhou University, Zhengzhou 450000, China

[6] China Institute of Intelligent Sensing, Zhengzhou University, Zhengzhou 450000, China

*Corresponding author: guobiao.hu@ntu.edu.sg

Abstract

This paper proposes harnessing the aerokinetic energy in flue systems and it explores the effect of the ash deposition on flow-induced vibration energy harvesting performance. Bell-shaped and horn-like bluff bodies are designed to simulate different ash depositions on a conventional elliptic cylinder bluff body. Wind tunnel experiments were conducted to investigate the energy harvesting performance using different ash deposition distributed over the bluff bodies. The experimental results show that compared to the baseline model of a conventional elliptic cylinder bluff body, the bell-shaped bluff body suppresses the flow-induced vibration and deteriorates the energy harvesting performance. In contrast, the horn-like bluff body can benefit energy harvesting by reducing the galloping cut-in wind speed and increasing the voltage output. The voltage output of an optimal prototype using the horn-like bluff body is increased by 516%. Computational fluid dynamics (CFD) simulations were carried out to unveil the physical mechanisms behind the phenomena. The CFD analysis results indicate that the appearance of the small-scale secondary vortices (SV) widens the wake flow and increases the aerodynamic force produced by the horn-like bluff body. The flow-induced vibration of the harvester using the horn-like bluff body transforms from VIV to galloping. Therefore, it has been preliminarily demonstrated that the unfavorable ash deposition phenomenon in flue systems has the potential for promoting flow-induced vibration energy harvesting.

Keywords: ash deposition, energy harvesting, flow-induced vibration, galloping vortex-induced vibration

1. Introduction

In recent years, low-power consumption devices have been massively used in various fields to develop the Internet of Things (IoTs) [1, 2]. Most of these devices are powered by traditional chemical batteries. However, they often have limited storage capacities but bulky volumes. In some particular scenarios, such as remote areas, underwater environments, implant health monitoring, batteries are difficult to replace and maintain [3]. Therefore, harvesting energy from the ambient environment to provide the necessary power supply becomes a suitable battery-free solution to address the above issue. Common natural sources that are widely accessible in our ambient environment include solar energy [4, 5], vibration energy [6], wind energy [7, 8], and wave energy [9, 10]. Vibration energy harvesting refers to the technique of converting vibration energy into electrical energy through piezoelectric [11-13], electromagnetic [14, 15], or electrostatic [16, 17] transduction mechanisms. Due to the advantages of high power density, simple structure, and long service life, piezoelectric energy harvesting has attracted lots of research interest [18, 19].

Flow-induced vibration (FIV) is a natural phenomenon that ubiquitously exists in our ambient environment. Therefore, FIV-based energy harvesting technology has been extensively developed in recent years [20]. FIV phenomena can be further classified into vortex-induced vibration (VIV) [21], galloping [22], flutter [23, 24], and wake galloping [25]. VIV-based piezoelectric energy harvesters (VIVPEH) can efficiently generate considerable power in the lock-in region. However, when the flow velocity exceeds the lock-in region, the structural vibration will decrease significantly, and the energy harvesting performance will deteriorate dramatically. Researchers have devoted numerous efforts to improving the performance of VIVPEH. Akaydin *et al*. [26] designed a VIVPEH by connecting a cantilever beam to a cylindrical bluff body. The wind tunnel test showed that the designed VIVPEH could generate approximately a power of 0.1 mW at a wind speed of 1.192 m/s. Dai *et al*. [27] established a nonlinear distributed-parameter model for a VIVPEH. They discussed the influences of the bluff body, the piezoelectric sheet length, and the electrical resistance on the synchronization region and the performance of the harvester. Azadeh-Ranjba *et al*. [28] investigated the influence of the aspect ratio of the rigid cylinder on a VIVPEH. The results indicated that an appropriate aspect ratio could not only increase the power output of the VIVPEH but also broaden its lock-in region. In recent years, researchers have been showing interest in optimizing the surface structure of the bluff body to widen the lock-in region of a VIVPEH for broadband energy harvesting. For example, Hu *et al*. [29] added two rods to a circular cylinder bluff body of a VIVPEH to alter the aerodynamic forces, thereby widening the wind speed range for energy harvesting. Wang *et al*. [30] introduced the metasurface concept in the design of a VIVPEH for the first time. The results demonstrated that by decorating the circular cylinder bluff body with a suitable metasurface, the synchronization region of the VIVPEH can be enlarged by 63.64%. Furthermore, the voltage output amplitude can also be remarkably increased.

Unlike VIVPEHs, galloping-based piezoelectric energy harvesters (GPEHs) are not restricted by lock-in region and can realize energy harvesting at higher wind speeds. Regarding the underlying mechanism of galloping, some fundamental studies can be found in the following literature. Den Hartog [31] provided an early explanation of the galloping vibration of a transmission line due to the action of a transverse wind. Scruton [32] employed statistical concepts to estimate dynamic responses caused by random fluctuations in atmospheric wind speed. Parkinson [33, 34] developed an analytical model based on quasi-steady approximation and successfully predicted the galloping amplitude of a square-section bluff body. More extensive discussions on this subject can be found in the books [35, 36]. Recently, the research of GPEHs has attracted lots of interest. Barrero-Gil *et al*. [37] developed a lumped parameter model to describe and predict the dynamics of a GPEH. Sirohi *et al*. [38] theoretically and experimentally studied a GPEH with a D-shaped cross-section bluff body. The results showed that when the wind speed was 10.5 miles per hour, the maximum power produced by the GPEH could reach 1.14 mW. Abdelkefi *et al*. [39] designed a GPEH with a square-section bluff body and investigated the influence of Reynolds number on its cut-in wind speed and output power. The results revealed that load resistance and Reynolds number play a crucial role in affecting the output power. Wang *et al*. [40] used metasurfaces in designing the square-section bluff body of a GPEH. It was found that the maximum output voltage of the GPEH with a square-section bluff body wrapped on the convex cylindrical metasurface was increased by more than 20%.

Heat exchangers are the essential devices to realize heat transfer in refrigeration, air conditioning, power stations, chemical plants, etc. However, the ash deposition of dusty flue gas in the boiler and heat exchanger often threatens the safety of the equipment and affects the heat exchange performance. Therefore, a lot of research on the ash deposition phenomenon in heat exchangers has been carried out. Han *et al*. [41] studied the ash deposition on the surface of a tube-row heat exchanger. They also analyzed the influence of the particle size, the flow rate, and the tube bank shape on the ash deposition phenomenon. Bouris *et al*. [42] investigated the drop-shaped arrangement of tube bundles. The results indicated that while the heat transfer coefficient of the tube bundles was increased, the particle deposition rate and the pressure drop were reduced by 75% and 40%, respectively. Mavridou *et al*. [43] employed numerical methods to calculate the particle deposition and evaluate the heat transfer performance of circular tubes with various diameters. Compared to the standard configuration, the particle deposition rate decreased by 30%, and the heat transfer per unit volume increased by 28%. However, ash deposition in the flue might not always have a negative effect. The cross-section shape of the heat exchange tube will be changed as the ash deposition is formed. Considering the flow field environment in the flue gas tube, these factors have significant research value in FIV-based piezoelectric energy harvesting (FIVPEH). Therefore, this paper examines the ash deposition effect on FIVPEH for the first time. According to the cross-section shape of the heat exchanger tube under the effect of ash deposition, two new bluff body shapes, namely bell-shaped and horn-shaped, are designed. The ash deposition lengths are varied to simulate the variation of the pipe shape at different ash deposition times. Subsequently, the ash deposited FIVPEHs are comprehensively studied, including performance comparison, parameter analysis, and flow field analysis through wind tunnel experiments and CFD simulation.

2. Design concepts and experiment setup

2.1 Design concepts

During the combustion process, the high temperature in a furnace causes inorganic substances to undergo complex physical and chemical reactions, turning them into gases, liquids, and solids. All of them exist in the flue gas pipeline in the form of fly ash. Ash is formed due to the deposition of those inorganic materials in solid fuels after combustion [44]. When the flue gas flows through the heat exchanger, fly ash will deposit on the surface of the heat exchange tube. Because the fly ash in the flue gas pipe has a variety of physical states and the particle size of the ash particles ranges from nanometers to micrometers, there are several types of deposition mechanisms [45], including thermophoresis, inertial impaction, and eddy impaction. The ash deposition formed due to the first two mechanisms is usually located on the windward side of the tube. The ash deposition due to eddy impaction is often formed on the leeward side of the tube since the ash particles are too slight to separate from the flue gas flow and follow the airflow to the leeward side of the tube. Due to the eddy disturbance generated by the flow around the bluff body, the fly ash always deposits on the backside of the tube [46]. The schematic diagram of a general ash deposition process is shown in **Fig. 1**.

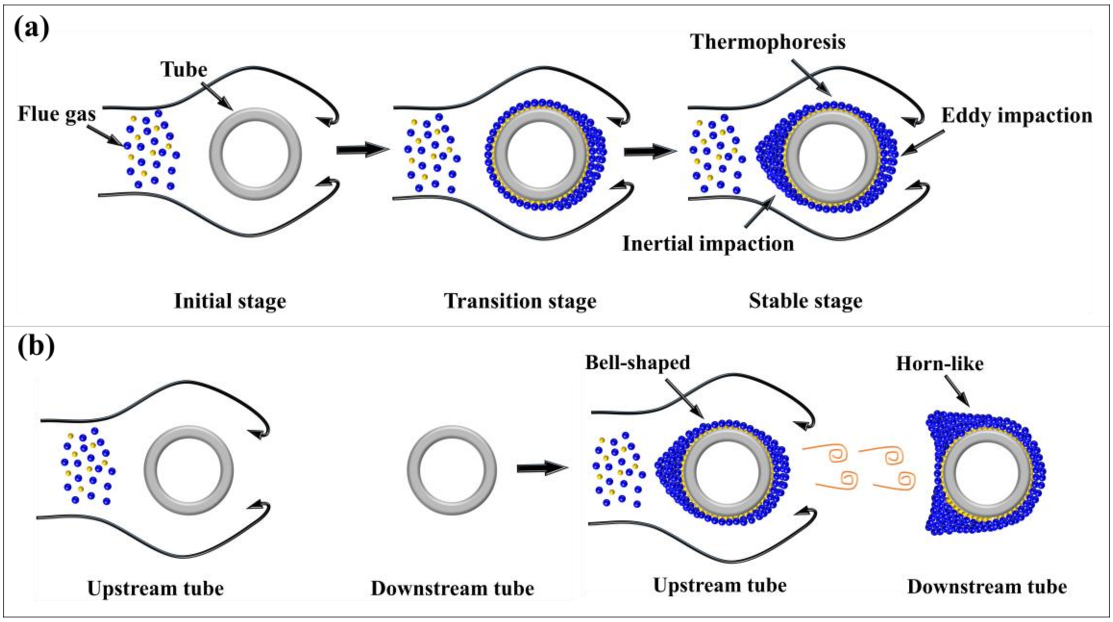

Fig. 1. (a) Schematic diagram of the three-stage process of ash deposition formation on a tube in heat exchange systems; (b) Schematic diagram of ash deposition shapes formed on multi-tubes in heat exchange systems.

Inspired by the deposition behavior of ash particles on the tube surface, this paper proposes to install a flow-induced piezoelectric energy harvester (FIVPEH) in the flue where aerokinetic energy exists. Ash deposition on the elliptic cylinder bluff body is considered, and its effect on the energy harvesting performance is investigated. Various shapes of ash depositions might lead to different aerodynamic characteristics of the bluff body. Therefore, two bluff bodies with differently shaped ash depositions are designed. **Fig. 2** exhibits the schematic diagram of the two FIVPEHs with different ash deposition attached to the bluff bodies. According to the geometric profile, the bluff bodies presented in **Fig. 2** (a) and (b) are referred to as bell-shaped and horn-like bluff bodies, respectively. According to the literature [44, 45], for a number tubes placed in series in the heat exchange system, the bell-shaped ash deposition is formed only on the first tube. Due to the influence of the wake of the upstream tube, horn-shaped ash depositions are formed on the remaining tubes. Both shapes of ash deposition are present in practice. In order to achieve a FIVPEH with a bell-shaped bluff body, one can install the FIVPEH in the front of all the tubes in the heat exchange system. To obtain a FIVPEH with a horn-shaped bluff body, one can install the FIVPEH at least after the first tube.

Each FIVPEH consists of a bluff body, a cantilever beam, and a piezoelectric transducer. The height of the bluff body is H. The length, width, and thickness of the cantilever beam are L, W, and T_b, respectively. **Fig. 2** (c) shows the key parameters that determine the geometric profiles of the bell-shaped and horn-like bluff bodies. Each bluff body is composed of a principal elliptic cylinder and one/two segmented ellipses. The segmented ellipse is an imitation of the ash deposition. The major and minor axes of the principal ellipse are a_1 and b_1, and $a_1 \times b_1$ = 30 mm × 20 mm. The major and minor axes of the segmented ellipse are a_2 and b_2, and $a_2 \times b_2$ = 24 mm × 10 mm. For the bell-shaped bluff body, the major axes of the principal ellipse and the segmented ellipse are on the same horizontal line. The distance between the left ends of the two ellipses is d_1. Considering that ash deposition may gradually grow, four bell-shaped bluff bodies with different ash deposition sizes are investigated by increasing d_1 from 3 mm to 12 mm with a step of 3 mm. For the horn-like bluff body, the two segmented ellipses are installed symmetrically on the two sides of the major axis of the principal ellipse. The angle between the major axes a_1 and a_2 is 45°. The distance from the end of the segmented ellipse to the edge of the principal ellipse is d_2. Similarly, four different d_2 (3 mm, 6 mm, 9 mm, and 12 mm) are selected to simulate the ash deposition growth.

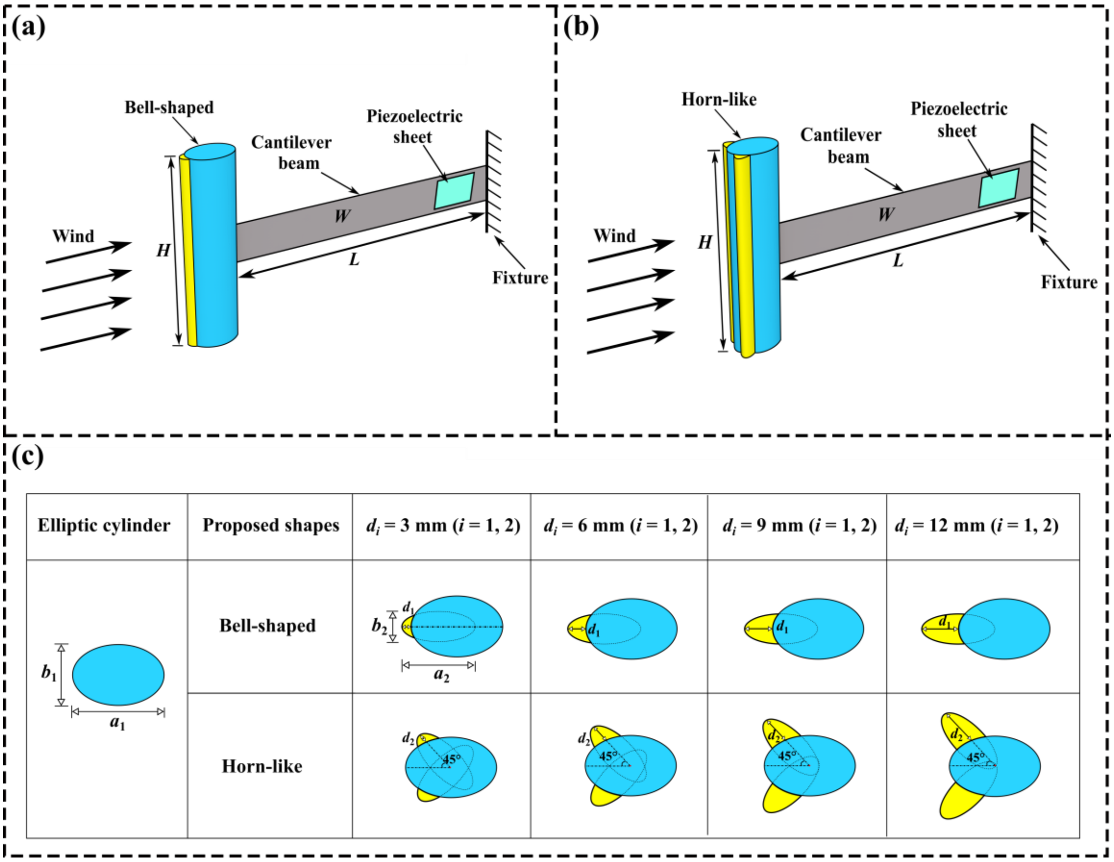

Fig. 2. Schematics of PEHs with different ash depositions: (a) bell-shaped ash deposition; (b) horn-like ash deposition; (c) geometries of the ash deposited bluff bodies.

2.2 Experimental setup

Fig. 3 presents the experimental setup and the physical prototypes of the PEH with bell-shaped and horn-like bluff bodies. A PEH with an ordinary bluff body without ash deposition is used as the baseline model for comparison. In the experiment, the PEHs are, separately, placed in an open wind tunnel with a diameter of 400 mm. The turbulence intensity is controlled to be less than 1.0 %. The bluff body is made of rigid foam material. The major axis, the minor axis, and the height of the elliptic cylinder bluff body are 30 mm, 20 mm, and 118 mm, respectively. The cantilever beam is made of aluminum, and its dimensions are $L \times W \times T_b$ = 184 mm × 25 mm × 0.5 mm. The capacitance C_p of the piezoelectric transducer (PZT-5, Jiaye-shi

Co, China) is 24.87 nF. The wind speed in the wind tunnel is controlled by a draught fan and is measured by a hot-wire anemometer (405i, Testo Company, USA). The two-stage honeycomb device straightens the wind generated by the draught fan. The wind speed range investigated in this paper is from 0.87 m/s to 3.61 m/s. The natural frequencies of all the PEHs are calibrated to be almost the same, approximately 8.0 Hz. The displacements of the bluff bodies are measured by a laser displacement sensor (Panasonic: HG-C1400) with a resolution of 300 μm. The signals are recorded using a dual-channel USB data acquisition instrument (USB DAQ-280G). The voltage generated by the piezoelectric transducer is recorded by a data acquisition apparatus (DS1104S, RIGOL, China).

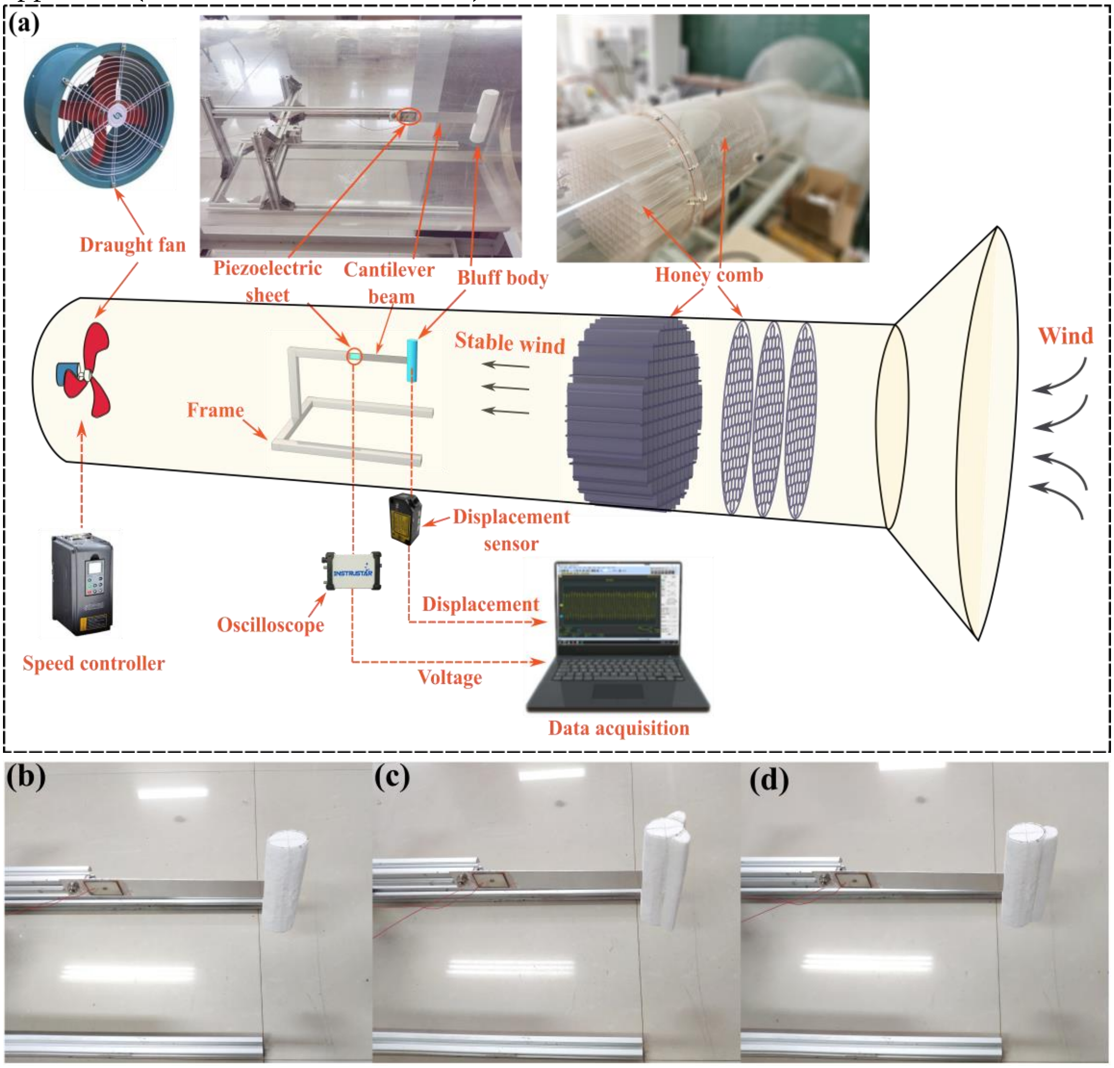

Fig. 3. (a) The experimental setup; (b) the fabricated baseline PEH; (c) the fabricated PEH with the horn-like bluff body; (d) the fabricated PEH with the bell-shaped bluff body.

3. Results and discussion

3.1 The elliptic cylinder bluff body

The wind tunnel test results of the PEH with the elliptic cylinder bluff body are illustrated in **Fig. 4** and **Fig. 5**. **Fig. 4** (a) and (b) present the output voltage and vibration amplitude responses, respectively. A lock-in region, with lower and upper bounds of 1.41 m/s and 2.51 m/s, is observed in the response diagram. It indicates that the PEH with the elliptic cylinder bluff body exhibits VIV. Over the lock-in region, with the increase of wind speed, the output voltage from the PEH first increases, then decreases. A maximum voltage of 2.33 V is obtained when the wind speed reaches 1.82 m/s. When the wind speed exceeds 2.51 m/s beyond the lock-in region, the voltage output becomes negligibly small. The displacement response of the PEH presented in **Fig. 4** (b) exhibits a similar behavior. Appreciable vibration of the PEH occurs only within the lock-in region. The vibration amplitude reaches a maximum value of 7.06 mm at the wind speed of 2.51 m/s.

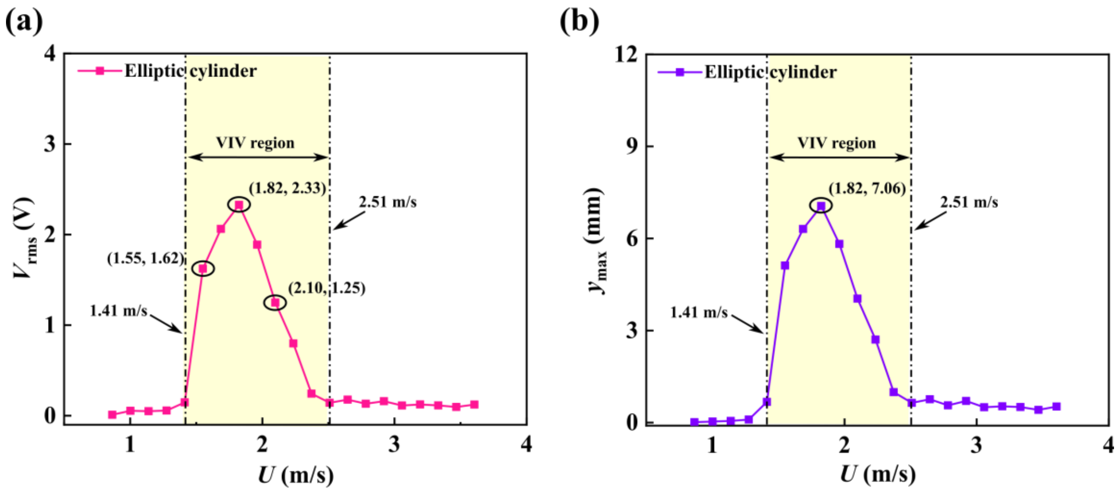

Fig. 4. Results of the PEH with elliptic cylinder bluff body: (a) RMS voltage output (b) maximum vibration displacement of the bluff body.

Fig. 5 exhibits the dominant vibration frequency of the PEH in the VIV region, and the voltage time-history is plotted at the wind speeds of 1.55 m/s, 1.82 m/s, and 2.10 m/s. The three wind speeds are, respectively, taken from the initial excitation branch, upper branch, and lower branch of the VIV region. In **Fig. 5** (a), it is noted that the dimensionless frequency gradually increases to 1 as the wind speed increases, then keeps growing as the wind speed increases. However, the frequency shift in the lock-in region is minor, and the frequency ratio is always around 1. This phenomenon agrees with the results in the literature [47]. Thus, it further proves that the PEH with the elliptic cylinder bluff body performs VIV. It can be seen from **Fig. 5** (b) that at all the three wind speeds, the PEH undergoes harmonic vibration. Due to the locking phenomenon, the output voltage of the PEH at the wind speed of 1.82 m/s is obviously larger than that when the wind speed is changed to 1.55 m/s or 2.10 m/s.

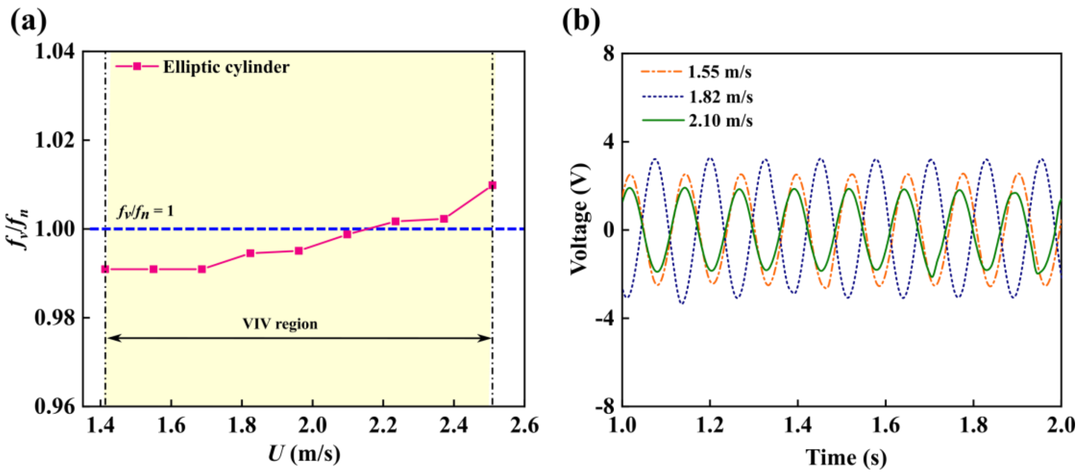

Fig. 5. (a) The dominant non-dimensional frequency of the PEH with elliptic cylinder bluff body under different wind speeds. (b) the voltage output time histories at the wind speeds 1.55 m/s, 1.82 m/s, and 2.10 m/s.

3.2 The Bell-shaped bluff body

As seen in **Fig. 6**, the bell-shaped additions produce a decrease in the amplitude of motion and a reduction of the voltage generated. For the PEH with the elliptic cylinder bluff body, the VIV phenomenon occurs over the wind speed range U = 1.41 m/s ~ 2.51 m/s. A maximum output voltage of 2.33 V is obtained at the wind speed of 1.82 m/s. For the PEH with the bell-shaped bluff body, for d_1 equal to 3 mm, 6 mm, 9 mm, and 12 mm, the maximum voltage correspondingly becomes 0.99 V, 0.77 V, 0.44 V, and 0.49 V, and the maximum amplitude is 3.35 mm, 2.93 mm, 1.75 mm, and 1.79 mm, respectively. In other words, bell-shaped bluff bodies are not beneficial for energy harvesting. In contrast, they demonstrate the potential application for suppressing galloping-induced vibrations. Moreover, optimizing the parameters of the bell-shaped bluff body may lead to a maximum suppression performance. For instance, in the above case studies, the bell-shaped bluff body with d_1 = 9 mm shows the strongest vibration suppression effect: its maximum amplitude is reduced by 75%, compared to the baseline model.

The time history responses of the PEH with the bell-shaped bluff body (d_1 = 9 mm) at U = 1.41 m/s are presented in **Fig. 6** (c) and (d). The results of the baseline model at U = 1.82 m/s are also presented for comparison. U = 1.41 m/s and 1.82 m/s are the optimal wind speeds to achieve the maximum voltage output for each case. Both cases exhibit harmonic vibration, while the baseline model has a significantly larger vibration amplitude, which is consistent with the results in **Fig. 6** (a) and (b).

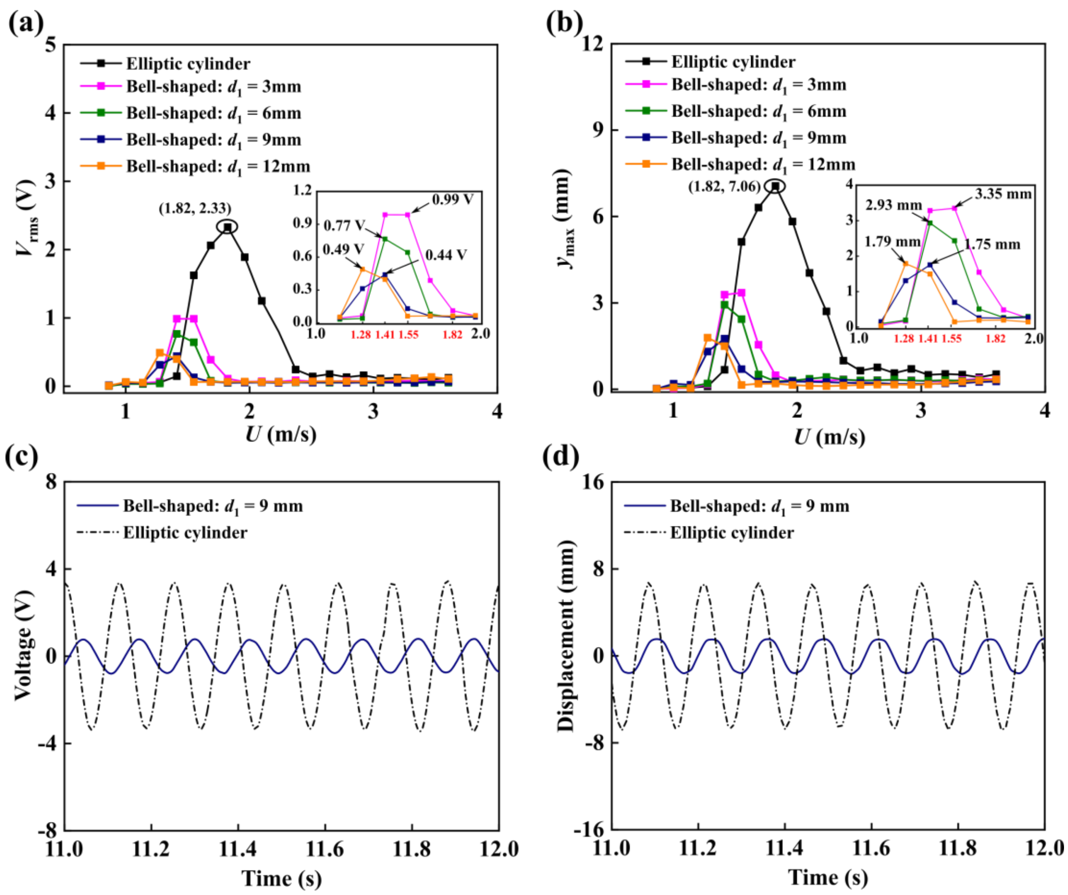

Fig. 6. Performance comparison of the PEHs with different bluff bodies: (a) RMS voltage outputs; (b) maximum vibration displacement of the bluff bodies; (c) time-history voltage output and (d) displacement of the PEHs with the bell-shaped bluff body under the optimal wind speed of U = 1.41 m/s and the elliptic cylinder bluff body under the optimal wind speed of U = 1.82 m/s.

3.3 The Horn-like bluff body

The results of the PEH with the horn-like bluff body of varying d_2 are presented in **Fig. 7**. The results of the baseline model are also provided for comparison. **Fig. 7** (a) clearly shows that, unlike the baseline model, the PEH with the horn-like bluff body mainly exhibits the galloping phenomenon, regardless of the values of d_2. Hence, the PEH with the horn-like bluff body can produce significant voltage outputs over a much wider wind speed range. Moreover, unlike the behavior in the VIV region of the baseline model, with the increase of the wind speed, the voltage output monotonically increases. Over the wind speed range under investigation, for d_2 equal to 3 mm, 6 mm, 9 mm, and 12 mm, the maximum voltage output of the PEH with the horn-like bluff body correspondingly becomes 14.06 V, 14.36 V, 14.20 V, and 14.24 V, which are much larger than that of the baseline model (2.33 V). **Fig. 7** (b) compares the displacement response of the PEH with the horn-like bluff body. For d_2 equal to 3 mm, 6 mm, 9 mm, and 12 mm, the maximum displacement of the PEH with the horn-like bluff body becomes 49.96 mm, 56.32 mm, 54.45 mm, and 55.46 mm, which indicate 607%, 697%, 671%, and 685% increases compared to the baseline model. Among the above cases, using the horn-like bluff body with d_2 of 6 mm leads to the best performance. Its maximum voltage output is increased by 516% compared to the baseline model. In addition, the cut-in wind speed of the optimal design, i.e., d_2 = 6 mm, is about 1.28 m/s, which is smaller by 9% compared to the baseline model. Therefore, using the horn-like bluff body is also favorable for low wind speed energy harvesting.

In fact, the significant increase of the voltage output is the consequence of the galloping phenomenon. And the low cut-in wind speed advantage is inherited from the VIV behavior. In the enlarged views in **Fig. 7** (a) and (b), it is noted that over the wind range 1.1 m/s ~ 1.8 m/s, when d_2 = 3 mm or 6 mm, the PEH with the horn-like bluff body undergoes VIV: the voltage/displacement response first increases, then decreases. When d_2 = 9 mm or 12 mm, the VIV phenomenon appears in the wind speed range of 1.28 m/s ~ 1.69 m/s. The time-history responses of the optimal design (d_2 = 6 mm) at U = 1.82 m/s, which is the optimal wind speed of the baseline model, are presented in **Fig. 7** (c) and (d). It can be seen in **Fig. 7** (a) that both cases exhibit harmonic vibration. Even U = 1.82 m/s is the optimal wind speed of the baseline model, while not for the PEH with the horn-like bluff body; the voltage and displacement responses of the PEH with the horn-like bluff body are still larger than those of the baseline model. In brief, the PEH with the horn-like bluff body demonstrates a superior wind energy harvesting ability.

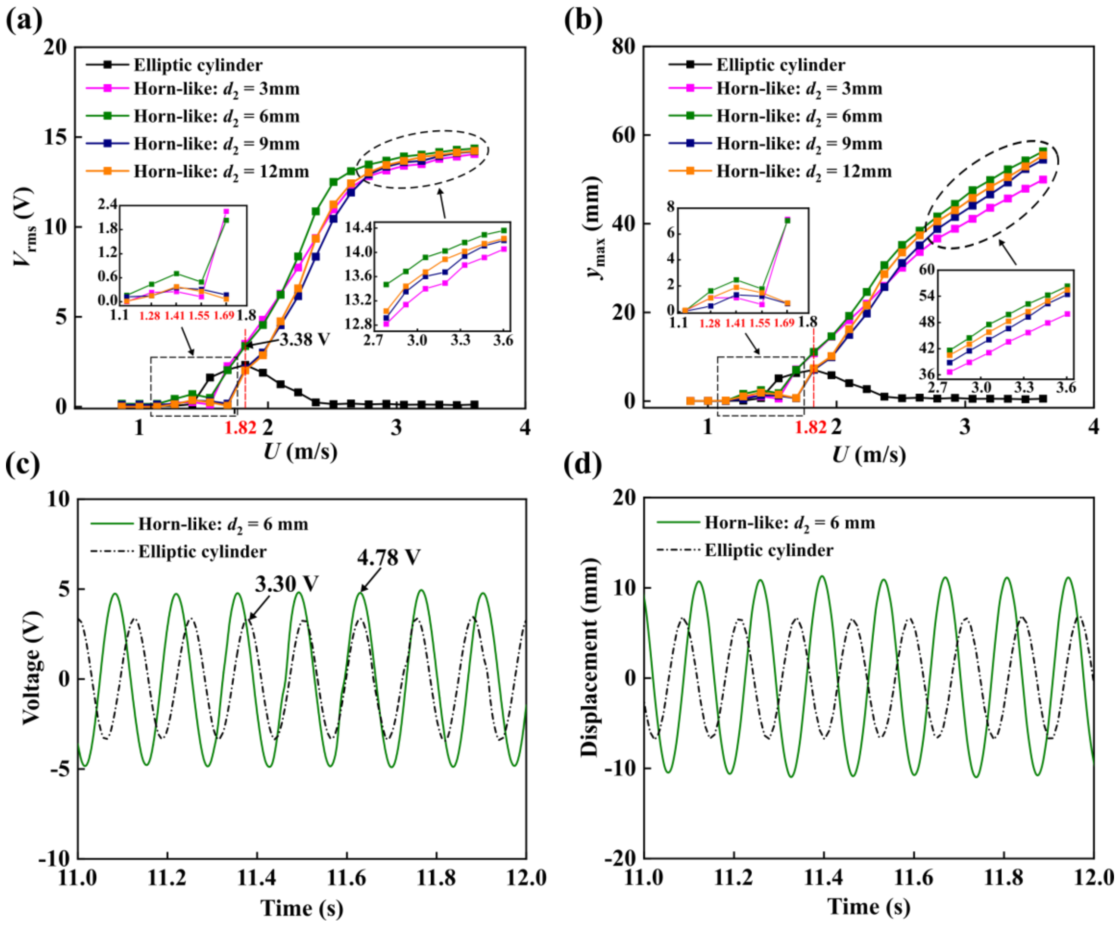

Fig. 7. Performance comparison of the PEHs with different bluff bodies: (a) RMS voltage outputs;

(b) maximum vibration displacement of the bluff bodies; (c) time-history voltage output and (d) displacement of the PEHs with the horn-like bluff body and the elliptic cylinder bluff body under the wind speed of $U = 1.82$ m/s.

4. Interpretation based on CFD simulation

Computational fluid dynamics (CFD) simulations are carried out to further reveal the effect of ash deposition on the aerodynamics of the bluff body. CFD models are built using the commercial software XFlow, which adopts the lattice Boltzmann method. The dimensions of the bluff bodies in simulations are consistent with those of the physical prototypes tested in the experiments. The calculation domain set in the simulation is a rectangle with a length of $40b_1$ and a width of $20b_1$, where b_1 is the length of the minor axis of the principal ellipse of the bluff body. The left and right boundary conditions of the calculation domain are set as velocity inlet and flow outlet, respectively. The fluid is air. The upper and lower boundary conditions are set to be walls. The distance between the center of the bluff body and the upper boundary is $10b_1$, and that to the outlet boundary is $30b_1$ to ensure that the flow field behind the bluff body can be fully developed. In the CFD simulations, the external single-phase forced incompressible model is selected to simulate the flow. The time step is automatically fixed to 5×10^{-5} s. The Reynolds number of the simulated flow field is approximately 2460.

As known from the results presented in the previous section, using the bell-shaped bluff body leads to vibration suppression and a deteriorated energy harvesting performance. On the contrary, using the horn-like bluff body induces the galloping phenomenon and significantly improves the energy harvesting performance. **Fig. 8** presents the vorticity contours of the bell-shaped (d_1 = 9 mm), elliptic cylinder, and horn-like (d_2 = 6 mm) bluff bodies at different time stages to reveal the aerodynamic mechanisms behind the above conclusion. From **Fig. 8**, one can find that for the bell-shaped bluff body, the presence of a small elliptical bulge in the front streamlines the oncoming flow over the bluff body. Thus, the vortex shedding is similar to that of the elliptic cylinder bluff body: in both cases, primary large-scale vortices (PV) are produced behind the bluff bodies. The width of the wake is evaluated to indicate the intensity of the vortex shedding. The widths of the wake produced after the bell-shaped and elliptic cylinder bluff bodies are $1.57b_1$ and $1.79\ b_1$, respectively. This implies that the intensity of the vortex shedding of the bell-shaped bluff body is weaker than that of the elliptic cylinder. This explains why the vibration amplitude of the bell-shaped bluff body is smaller than that of the elliptic cylinder one. Unlike the elliptic cylinder bluff body, for the horn-like one, due to the presence of two small elliptical bulges, not only primary large-scale vortices (PV), but also small-scale secondary vortices (SV) are produced in the wake flow. Because of the interaction between PV and SV, the vortex shedding effect is delayed, resulting in a significant increase of the wake vortices. Moreover, it is observed that the wake width of the horn-like bluff body is much wider than that of the elliptic cylinder one, which indicates a stronger aerodynamic instability in the wake. Therefore, unlike the vibration mode of the elliptic cylinder bluff body, the vibration mode of the horn-like bluff body is galloping, which can induce a larger-amplitude vibration and produce a higher voltage output. In summary, the formation of small-scale secondary vortices (SV) plays a key role in the intensity of vibration.

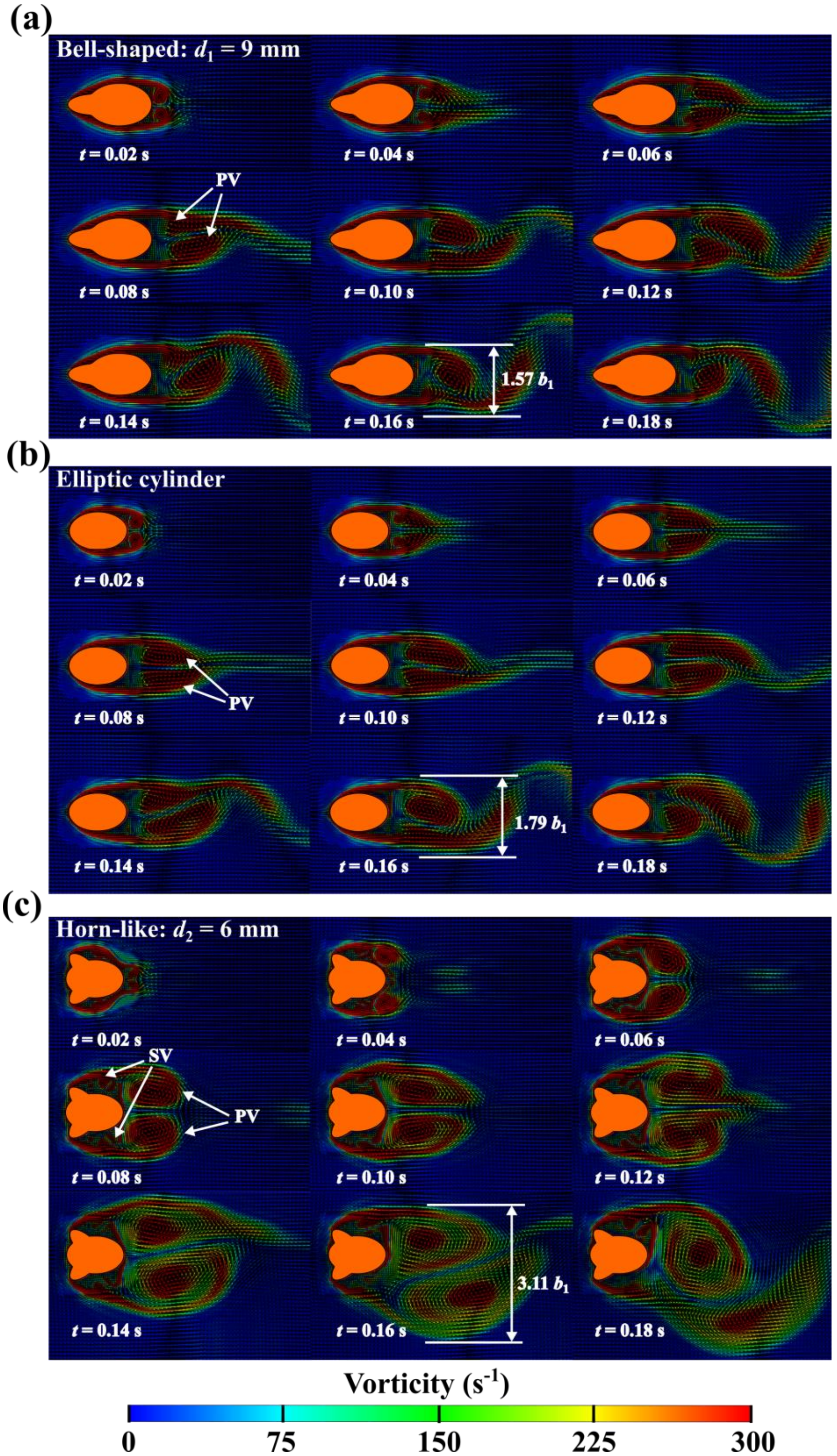

Fig. 8. Comparison of flow-field evolution with time for the three bluff bodies at the wind speed

of U = 1.82 m/s: (a) the bell-shaped (d_1 = 9 mm) bluff body; (b) the elliptic cylinder bluff body; (c) the horn-like (d_2 = 6 mm) bluff body.

The pressure contours around the bell-shaped (d_1 = 9 mm), elliptic cylinder, and horn-like (d_2 = 6 mm) bluff bodies at the wind speed of 1.82 m/s are shown in **Fig. 9**. Obviously, it can be observed that the low-pressure region around the horn-like bluff body is significantly larger than those around the other two bluff bodies. The larger pressure difference causes the horn-like bluff body to vibrate more violently than the other two bluff bodies. Comparing the bell-shaped and elliptic cylinder bluff bodies, the low-pressure region around the bell-shaped bluff body is smaller than that around the elliptic cylinder bluff body. Therefore, the bell-shaped bluff body undergoes the smallest vibration. **Fig. 10** presents the velocity contours of the bell-shaped (d_1 = 9 mm), elliptic cylinder, and horn-like (d_2 = 6 mm) bluff bodies at the wind speed of 1.82 m/s. The high-velocity region in **Fig. 10** corresponds to the low-pressure region in **Fig. 9**. The high-velocity region around the horn-like bluff body is the largest, which enhances the oscillation of the horn-like bluff body, and makes its vibration significantly higher than the other two bluff bodies. The above discussion agrees well with the conclusions obtained from the experiments in the previous section.

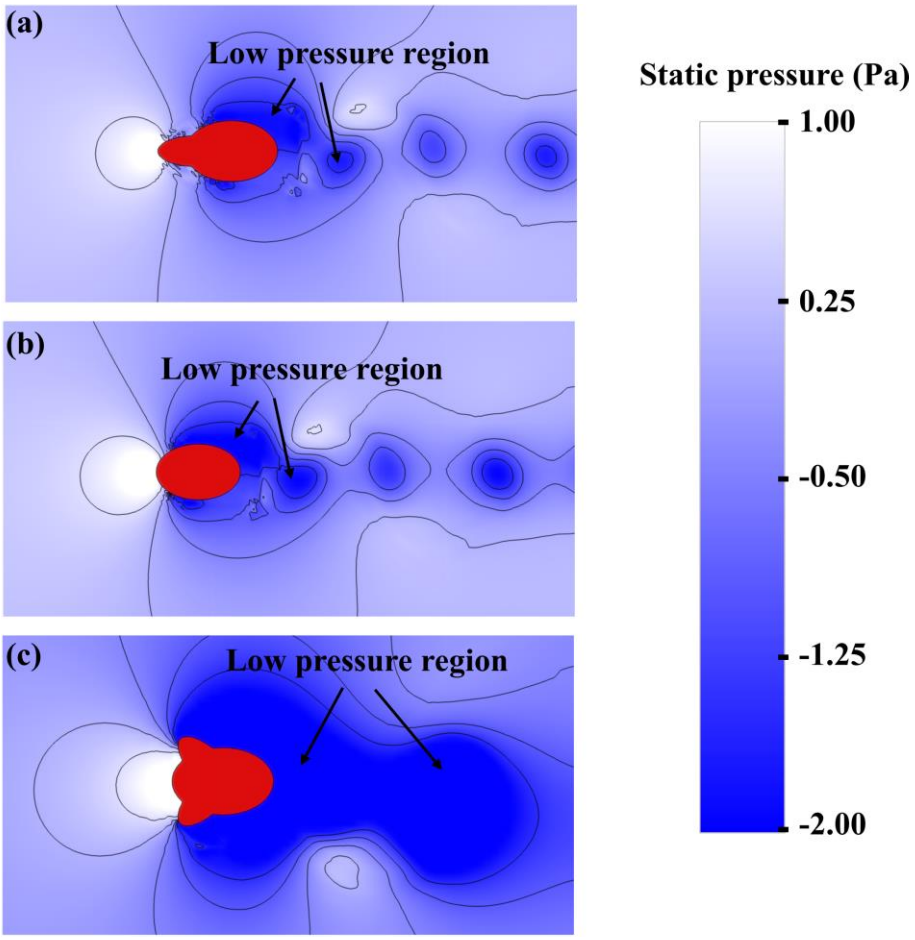

Fig. 9. Pressure contour around (a) the bell-shaped (d_1 = 9 mm) bluff body; (b) the elliptic cylinder bluff body; (c) the horn-like (d_2 = 6 mm) bluff body at the wind speed of 1.82 m/s.

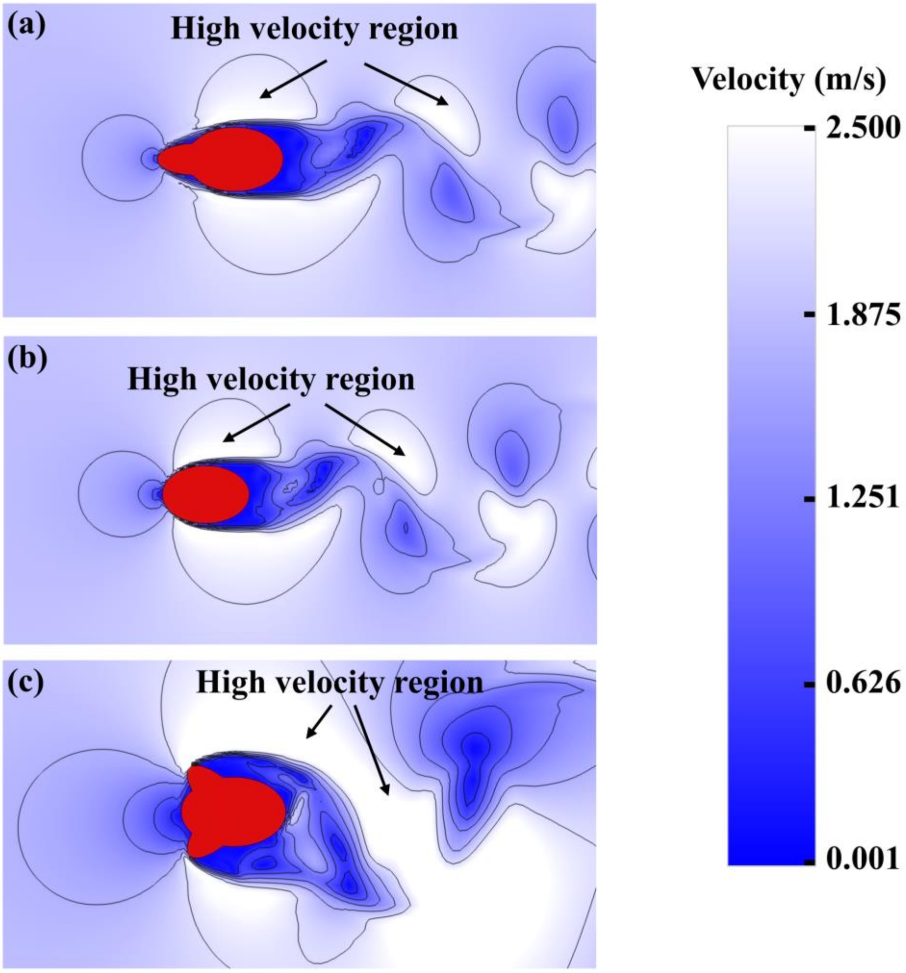

Fig. 10. Velocity contour around (a) the bell-shaped (d_1 = 9 mm) bluff body; (b) the elliptic cylinder bluff body; (c) the horn-like (d_2 = 6 mm) bluff body at the wind speed of 1.82 m/s.

5. Conclusion

This paper has explored the effect of ash deposition on flow-induced vibration energy harvesting in heat exchange systems. According to the shape and size of ash deposition, bell-shaped and horn-like bluff bodies have been proposed to simulate different ash depositions. Experimental results have revealed that the bell-shaped bluff bodies can suppress vibrations and are not beneficial for energy harvesting. In contrast, the horn-like bluff bodies can improve the energy harvesting performance by transforming VIV to galloping. The combination of VIV and galloping reduces the cut-in wind speed of the PEH and increases the voltage outputs under high wind speeds. The voltage output of an optimal prototype with d_2 = 6 mm has been increased by 516%. Besides, CFD simulations have been conducted to interpret the underlying mechanisms behind the phenomena. For the bell-shaped bluff body, a weaker aerodynamic force is generated because the wake width is smaller than that of the elliptic cylinder bluff body. Thus, the vibration of the bluff body is diminished. For the horn-like bluff body, due to the interaction of PV and SV, the wake width is increased, resulting in an increased aerodynamic force. The flow-induced vibration transforms from VIV to galloping. Therefore, a larger voltage output is generated by the PEH with the horn-like bluff body. In summary, a potential usefulness of the harmful ash deposition phenomenon in the flue gas pipeline for benefiting energy harvesting has been proposed and explored. Different ash deposition effects have been investigated. The work presented in this paper represents a preliminary study of the ash deposition effect on flow-induced vibration energy harvesting.

Acknowledgments

This work was supported by the National Natural Science Foundation of China (Grant No. 51977196), the China Postdoctoral Science Foundation (Grant No. 2020T130557), the Natural Science Foundation of Excellent Youth of Henan Province (Grant No. 222300420076), and the State Key Laboratory of Structural Analysis for Industrial Equipment, Dalian University of Technology, China (GZ21114).

References

[1] J. Wang, L. Geng, L. Ding, H. Zhu, D. Yurchenko, The state-of-the-art review on energy harvesting from flow-induced vibrations, Appl. Energy, 267 (2020) 114902.

[2] X.W. Fu, Y.S. Yang, Modeling and analysis of cascading node-link failures in multi-sink wireless sensor networks, Reliab. Eng. Syst. Saf., 197 (2020) 15.

[3] Z. Lai, S. Wang, L. Zhu, G. Zhang, J. Wang, K. Yang, D. Yurchenko, A hybrid piezo-dielectric wind energy harvester for high-performance vortex-induced vibration energy harvesting, Mech. Syst. Signal. Process., 150 (2021).

[4] C. Magazzino, M. Mele, N. Schneider, A machine learning approach on the relationship among solar and wind energy production, coal consumption, GDP, and CO2 emissions, Renew. Energ., 167 (2021) 99-115.

[5] J.J. Yoo, G. Seo, M.R. Chua, T.G. Park, Y.L. Lu, F. Rotermund, Y.K. Kim, C.S. Moon, N.J. Jeon, J.P. Correa-Baena, V. Bulovic, S.S. Shin, M.G. Bawendi, J. Seo, Efficient perovskite solar cells via improved carrier management, Nature, 590 (2021) 10.

[6] C.H. Li, S.C. Xu, J. Yu, Z. Li, W.F. Li, J.H. Wang, A.H. Liu, B.Y. Man, S.K. Yang, C. Zhang, Local hot charge density regulation: Vibration-free pyroelectric nanogenerator for effectively enhancing catalysis and in-situ surface enhanced Raman scattering monitoring, Nano Energy, 81 (2021) 10.

[7] J.L. Wang, S.H. Gu, C.Y. Zhang, G.B. Hu, G. Chen, K. Yang, H. Li, Y.Y. Lai, G. Litak, D. Yurchenko, Hybrid wind energy scavenging by coupling vortex-induced vibrations and galloping, Energy Convers. Manag., 213 (2020) 11.

[8] T. Morbiato, C. Borri, R. Vitaliani, Wind energy harvesting from transport systems: A resource estimation assessment, Appl. Energy, 133 (2014) 152-168.

[9] M.A. Mustapa, O.B. Yaakob, Y.M. Ahmed, C.K. Rheem, K.K. Koh, F.A. Adnan, Wave energy device and breakwater integration: A review, Renew. Sust. Energ. Rev., 77 (2017) 43-58.

[10] C. Chen, Z.Y. Liu, S.H. Wan, J.T. Luan, Q.Q. Pei, Traffic Flow Prediction Based on Deep Learning in Internet of Vehicles, IEEE Trans. Intell. Transp. Syst., 22 (2021) 3776-3789.

[11] H.S. Kim, J.-H. Kim, J. Kim, A review of piezoelectric energy harvesting based on vibration, International Journal of Precision Engineering and Manufacturing, 12 (2011) 1129-1141.

[12] F.K. Shaikh, S. Zeadally, Energy harvesting in wireless sensor networks: A comprehensive review, Renew. Sust. Energ. Rev., 55 (2016) 1041-1054.
[13] S. Fang, X. Fu, X. Du, W.-H. Liao, A music-box-like extended rotational plucking energy harvester with multiple piezoelectric cantilevers, Applied Physics Letters, 114 (2019).
[14] X. Zhao, J. Cai, Y. Guo, C. Li, J. Wang, H. Zheng, Modeling and experimental investigation of an AA-sized electromagnetic generator for harvesting energy from human motion, Smart. Mater. Struct., 27 (2018).
[15] K. Fan, Y. Zhang, S. E, L. Tang, H. Qu, A string-driven rotor for efficient energy harvesting from ultra-low frequency excitations, Appl. Phys. Lett., 115 (2019).
[16] Z. Yang, L. Tang, L. Yu, K. Tao, K. Aw, Modelling and analysis of an out-of-plane electret-based vibration energy harvester with AC and DC circuits, Mech. Syst. Signal. Process., 140 (2020).
[17] G. Hu, C. Zhao, Y. Yang, X. Li, J. Liang, Triboelectric energy harvesting using an origami-inspired structure, Appl. Energy, 306 (2022) 118037.
[18] J. Wang, S. Zhou, Z. Zhang, D. Yurchenko, High-performance piezoelectric wind energy harvester with Y-shaped attachments, Energy Conversion and Management, 181 (2019) 645-652.
[19] A. Abdelkefi, Aeroelastic energy harvesting: A review, International Journal of Engineering Science, 100 (2016) 112-135.
[20] L.B. Zhang, H.L. Dai, A. Abdelkefi, L. Wang, Improving the performance of aeroelastic energy harvesters by an interference cylinder, Appl. Phys. Lett., 111 (2017).
[21] K. Yang, T. Qiu, J. Wang, L. Tang, Magnet-induced monostable nonlinearity for improving the VIV-galloping-coupled wind energy harvesting using combined cross-sectioned bluff body, Smart Materials and Structures, 29 (2020).
[22] K. Yang, J.L. Wang, D. Yurchenko, A double-beam piezo-magneto-elastic wind energy harvester for improving the galloping-based energy harvesting, Appl. Phys. Lett., 115 (2019) 5.
[23] A. Abdelkefi, A.H. Nayfeh, M.R. Hajj, Modeling and analysis of piezoaeroelastic energy harvesters, Nonlinear Dyn., 67 (2011) 925-939.
[24] M. Bryant, E. Garcia, Modeling and Testing of a Novel Aeroelastic Flutter Energy Harvester, Journal of Vibration and Acoustics-Transactions of the Asme, 133 (2011) 011010.
[25] H. Wang, W. Yang, K.D. Nguyen, G. Yu, Wake-induced vibrations of an elastically mounted cylinder located downstream of a stationary larger cylinder at low Reynolds numbers, Journal of Fluids and Structures, 50 (2014) 479-496.
[26] H.D. Akaydin, N. Elvin, Y. Andreopoulos, The performance of a self-excited fluidic energy harvester, Smart. Mater. Struct., 21 (2012).
[27] H.L. Dai, A. Abdelkefi, L. Wang, Theoretical modeling and nonlinear analysis of piezoelectric energy harvesting from vortex-induced vibrations, J. Intell. Mater. Syst. Struct., 25 (2014) 1861-1874.
[28] V. Azadeh-Ranjbar, N. Elvin, Y. Andreopoulos, Vortex-induced vibration of finite-length circular cylinders with spanwise free-ends: Broadening the lock-in envelope, Physics of Fluids, 30 (2018).
[29] G. Hu, K.T. Tse, M. Wei, R. Naseer, A. Abdelkefi, K.C.S. Kwok, Experimental investigation on the efficiency of circular cylinder-based wind energy harvester with different rod-shaped attachments, Appl. Energy, 226 (2018) 682-689.
[30] J.L. Wang, S.K. Sun, L.H. Tang, G.B. Hu, J.R. Liang, On the use of metasurface for Vortex-Induced vibration suppression or energy harvesting, Energy Convers. Manag., 235 (2021) 14.
[31] J.P.D. Hartog, Transmission line vibration due to sleet, Transactions of the American Institute of Electrical Engineers, 51 (1932) 1074-1076.

[32] C. Scruton, Wind effects on structures, James Clayton Lecture, Proceedings Institution of Mechanical Engineers, 185 (1971) 301-317.

[33] G.V. Parkinson, Wind-induced instability of structures, Philosophical Transactions of the Royal Society of London, A269 (1971) 395-409.

[34] G.V. Parkinson, Phenomena and modelling of flow-induced vibrations of bluff bodies, Progress in Aerospace Sciences, 26 (1989) 169-224.

[35] R.D. Blevins, Flow-Induced Vibration, Van Nostrand Reinhold, New York, 1990.

[36] M.P. Païdoussis, S.J. Price, E. De Langre, Fluid-structure interactions: cross-flow-induced instabilities, Cambridge University Press, 2010.

[37] A. Barrero-Gil, G. Alonso, A. Sanz-Andres, Energy harvesting from transverse galloping, J. Sound Vibr., 329 (2010) 2873-2883.

[38] J. Sirohi, R. Mahadik, Harvesting Wind Energy Using a Galloping Piezoelectric Beam, Journal of Vibration and Acoustics-Transactions of the Asme, 134 (2012).

[39] A. Abdelkefi, M.R. Hajj, A.H. Nayfeh, Power harvesting from transverse galloping of square cylinder, Nonlinear Dynamics, 70 (2012) 1355-1363.

[40] J. Wang, S. Sun, G. Hu, Y. Yang, L. Tang, P. Li, G. Zhang, Exploring the potential benefits of using metasurface for galloping energy harvesting, Energy Convers. Manag., 243 (2021).

[41] H. Han, Y.-L. He, W.-Q. Tao, Y.-S. Li, A parameter study of tube bundle heat exchangers for fouling rate reduction, International Journal of Heat and Mass Transfer, 72 (2014) 210-221.

[42] D. Bouris, E. Konstantinidis, S. Balabani, D. Castiglia, G. Bergeles, Design of a novel, intensified heat exchanger for reduced fouling rates, International Journal of Heat and Mass Transfer, 48 (2005) 3817-3832.

[43] S.G. Mavridou, D.G. Bouris, Numerical evaluation of a heat exchanger with inline tubes of different size for reduced fouling rates, International Journal of Heat and Mass Transfer, 55 (2012) 5185-5195.

[44] S.-Z. Tang, Y.-L. He, F.-L. Wang, Y.-B. Tao, Parametric study on fouling mechanism and heat transfer characteristics of tube bundle heat exchangers for reducing fouling considering the deposition and removal mechanisms, Fuel, 211 (2018) 301-311.

[45] Y. Cai, K. Tay, Z. Zheng, W. Yang, H. Wang, G. Zeng, Z. Li, S. Keng Boon, P. Subbaiah, Modeling of ash formation and deposition processes in coal and biomass fired boilers: A comprehensive review, Appl. Energy, 230 (2018) 1447-1544.

[46] S.-Z. Tang, M.-J. Li, F.-L. Wang, Z.-B. Liu, Fouling and thermal-hydraulic characteristics of aligned elliptical tube and honeycomb circular tube in flue gas heat exchangers, Fuel, 251 (2019) 316-327.

[47] Navrose, S. Mittal, Lock-in in vortex-induced vibration, Journal of Fluid Mechanics, 794 (2016) 565-594.

REVISED Manuscript (marked or highlighted)

On the Investigation of Ash Deposition Effect on Flow-Induced Vibration Energy Harvesting

Junlei Wang[1], Shanghao Gu[1], Daniil Yurchenko[2], Guobiao Hu[3,4*], Ronghan Wei[5,6]

[1] School of Mechanical and Power Engineering, Zhengzhou University, Zhengzhou 450000, China

[2] Institute of Sound and Vibration Research, University of Southampton, Southampton, SO17 1BJ, UK.

[3] School of Civil and Environmental Engineering, Nanyang Technological University, 50 Nanyang Avenue, 639798, Singapore

[4] State Key Laboratory of Structural Analysis for Industrial Equipment, Dalian University of Technology, Dalian 116024, China

[5] School of Mechanics and Safety Engineering, Zhengzhou University, Zhengzhou 450000, China

[6] China Institute of Intelligent Sensing, Zhengzhou University, Zhengzhou 450000, China

*Corresponding author: guobiao.hu@ntu.edu.sg

Abstract

This paper proposes harnessing the aerokinetic energy in flue systems and it explores the effect of the ash deposition on flow-induced vibration energy harvesting performance. Bell-shaped and horn-like bluff bodies are designed to simulate different ash depositions on a conventional elliptic cylinder bluff body. Wind tunnel experiments were conducted to investigate the energy harvesting performance using different ash deposition distributed over the bluff bodies. The experimental results show that compared to the baseline model of a conventional elliptic cylinder bluff body, the bell-shaped bluff body suppresses the flow-induced vibration and deteriorates the energy harvesting performance. In contrast, the horn-like bluff body can benefit energy harvesting by reducing the galloping cut-in wind speed and increasing the voltage output. The voltage output of an optimal prototype using the horn-like bluff body is increased by 516%. Computational fluid dynamics (CFD) simulations were carried out to unveil the physical mechanisms behind the phenomena. The CFD analysis results indicate that the appearance of the small-scale secondary vortices (SV) widens the wake flow and increases the aerodynamic force produced by the horn-like bluff body. The flow-induced vibration of the harvester using the horn-like bluff body transforms from VIV to galloping. Therefore, it has been preliminarily demonstrated that the unfavorable ash deposition phenomenon in flue systems has the potential for promoting flow-induced vibration energy harvesting.

Keywords: ash deposition, energy harvesting, flow-induced vibration, galloping vortex-induced vibration

1. Introduction

In recent years, low-power consumption devices have been massively used in various fields to develop the Internet of Things (IoTs) [1, 2]. Most of these devices are powered by traditional chemical batteries. However, they often have limited storage capacities but bulky volumes. In some particular scenarios, such as remote areas, underwater environments, implant health monitoring, batteries are difficult to replace and maintain [3]. Therefore, harvesting energy from the ambient environment to provide the necessary power supply becomes a suitable battery-free solution to address the above issue. Common natural sources that are widely accessible in our ambient environment include solar energy [4, 5], vibration energy [6], wind energy [7, 8], and wave energy [9, 10]. Vibration energy harvesting refers to the technique of converting vibration energy into electrical energy through piezoelectric [11-13], electromagnetic [14, 15], or electrostatic [16, 17] transduction mechanisms. Due to the advantages of high power density, simple structure, and long service life, piezoelectric energy harvesting has attracted lots of research interest [18, 19].

Flow-induced vibration (FIV) is a natural phenomenon that ubiquitously exists in our ambient environment. Therefore, FIV-based energy harvesting technology has been extensively developed in recent years [20]. FIV phenomena can be further classified into vortex-induced vibration (VIV) [21], galloping [22], flutter [23, 24], and wake galloping [25]. VIV-based piezoelectric energy harvesters (VIVPEH) can efficiently generate considerable power in the lock-in region. However, when the flow velocity exceeds the lock-in region, the structural vibration will decrease significantly, and the energy harvesting performance will deteriorate dramatically. Researchers have devoted numerous efforts to improving the performance of VIVPEH. Akaydin *et al.* [26] designed a VIVPEH by connecting a cantilever beam to a cylindrical bluff body. The wind tunnel test showed that the designed VIVPEH could generate approximately a power of 0.1 mW at a wind speed of 1.192 m/s. Dai *et al.* [27] established a nonlinear distributed-parameter model for a VIVPEH. They discussed the influences of the bluff body, the piezoelectric sheet length, and the electrical resistance on the synchronization region and the performance of the harvester. Azadeh-Ranjba *et al.* [28] investigated the influence of the aspect ratio of the rigid cylinder on a VIVPEH. The results indicated that an appropriate aspect ratio could not only increase the power output of the VIVPEH but also broaden its lock-in region. In recent years, researchers have been showing interest in optimizing the surface structure of the bluff body to widen the lock-in region of a VIVPEH for broadband energy harvesting. For example, Hu *et al.* [29] added two rods to a circular cylinder bluff body of a VIVPEH to alter the aerodynamic forces, thereby widening the wind speed range for energy harvesting. Wang *et al.* [30] introduced the metasurface concept in the design of a VIVPEH for the first time. The results demonstrated that by decorating the circular cylinder bluff body with a suitable metasurface, the synchronization region of the VIVPEH can be enlarged by 63.64%. Furthermore, the voltage output amplitude can also be remarkably increased.

Unlike VIVPEHs, galloping-based piezoelectric energy harvesters (GPEHs) are not restricted by lock-in region and can realize energy harvesting at higher wind speeds. Regarding the underlying mechanism of galloping, some fundamental studies can be found in the following literature. Den Hartog [31] provided an early explanation of the galloping vibration of a transmission line due to the action of a transverse wind. Scruton [32] employed statistical concepts to estimate dynamic responses caused by random fluctuations in atmospheric wind speed. Parkinson [33, 34] developed an analytical model based on quasi-steady approximation and successfully predicted the galloping amplitude of a square-section bluff body. More extensive discussions on this subject can be found in the books [35, 36]. Recently, the research of GPEHs has attracted lots of interest. Barrero-Gil *et al*. [37] developed a lumped parameter model to describe and predict the dynamics of a GPEH. Sirohi *et al*. [38] theoretically and experimentally studied a GPEH with a D-shaped cross-section bluff body. The results showed that when the wind speed was 10.5 miles per hour, the maximum power produced by the GPEH could reach 1.14 mW. Abdelkefi *et al*. [39] designed a GPEH with a square-section bluff body and investigated the influence of Reynolds number on its cut-in wind speed and output power. The results revealed that load resistance and Reynolds number play a crucial role in affecting the output power. Wang *et al*. [40] used metasurfaces in designing the square-section bluff body of a GPEH. It was found that the maximum output voltage of the GPEH with a square-section bluff body wrapped on the convex cylindrical metasurface was increased by more than 20%.

Heat exchangers are the essential devices to realize heat transfer in refrigeration, air conditioning, power stations, chemical plants, etc. However, the ash deposition of dusty flue gas in the boiler and heat exchanger often threatens the safety of the equipment and affects the heat exchange performance. Therefore, a lot of research on the ash deposition phenomenon in heat exchangers has been carried out. Han *et al*. [41] studied the ash deposition on the surface of a tube-row heat exchanger. They also analyzed the influence of the particle size, the flow rate, and the tube bank shape on the ash deposition phenomenon. Bouris *et al*. [42] investigated the drop-shaped arrangement of tube bundles. The results indicated that while the heat transfer coefficient of the tube bundles was increased, the particle deposition rate and the pressure drop were reduced by 75% and 40%, respectively. Mavridou *et al*. [43] employed numerical methods to calculate the particle deposition and evaluate the heat transfer performance of circular tubes with various diameters. Compared to the standard configuration, the particle deposition rate decreased by 30%, and the heat transfer per unit volume increased by 28%. However, ash deposition in the flue might not always have a negative effect. The cross-section shape of the heat exchange tube will be changed as the ash deposition is formed. Considering the flow field environment in the flue gas tube, these factors have significant research value in FIV-based piezoelectric energy harvesting (FIVPEH). Therefore, this paper examines the ash deposition effect on FIVPEH for the first time. According to the cross-section shape of the heat exchanger tube under the effect of ash deposition, two new bluff body shapes, namely bell-shaped and horn-shaped, are designed. The ash deposition lengths are varied to simulate the variation of the pipe shape at different ash deposition times. Subsequently, the ash deposited FIVPEHs are comprehensively studied, including performance comparison, parameter analysis, and flow field analysis through wind tunnel experiments and CFD simulation.

2. Design concepts and experiment setup

2.1 Design concepts

During the combustion process, the high temperature in a furnace causes inorganic substances to undergo complex physical and chemical reactions, turning them into gases, liquids, and solids. All of them exist in the flue gas pipeline in the form of fly ash. Ash is formed due to the deposition of those inorganic materials in solid fuels after combustion [44]. When the flue gas flows through the heat exchanger, fly ash will deposit on the surface of the heat exchange tube. Because the fly ash in the flue gas pipe has a variety of physical states and the particle size of the ash particles ranges from nanometers to micrometers, there are several types of deposition mechanisms [45], including thermophoresis, inertial impaction, and eddy impaction. The ash deposition formed due to the first two mechanisms is usually located on the windward side of the tube. The ash deposition due to eddy impaction is often formed on the leeward side of the tube since the ash particles are too slight to separate from the flue gas flow and follow the airflow to the leeward side of the tube. Due to the eddy disturbance generated by the flow around the bluff body, the fly ash always deposits on the backside of the tube [46]. The schematic diagram of a general ash deposition process is shown in **Fig. 1**.

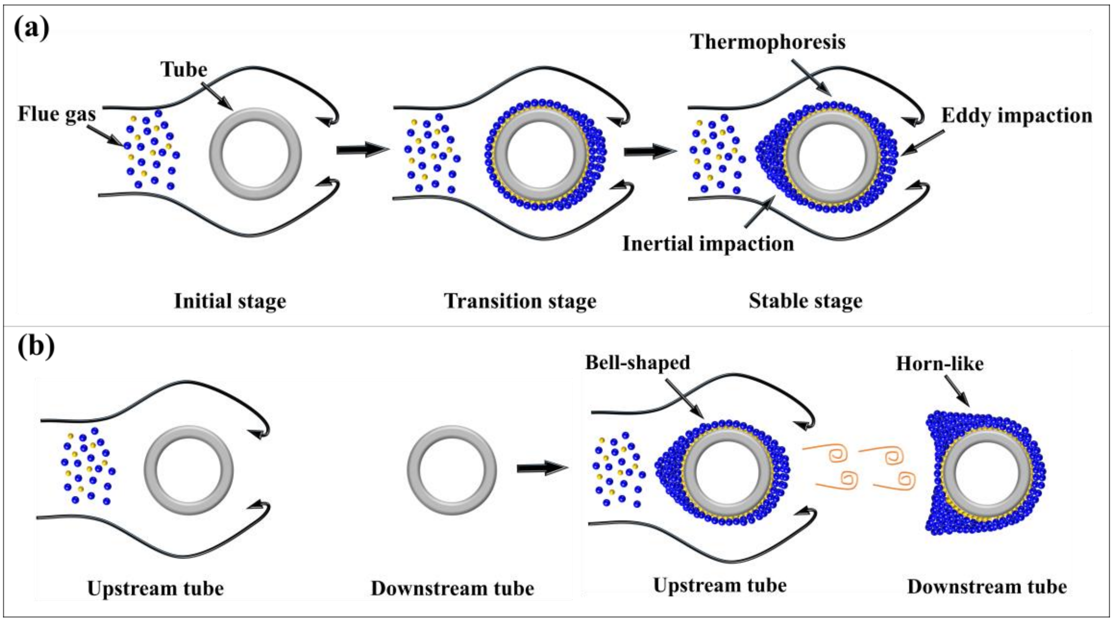

Fig. 1. (a) Schematic diagram of the three-stage process of ash deposition formation on a tube in heat exchange systems; (b) Schematic diagram of ash deposition shapes formed on multi-tubes in heat exchange systems.

Inspired by the deposition behavior of ash particles on the tube surface, this paper proposes to install a flow-induced piezoelectric energy harvester (FIVPEH) in the flue where aerokinetic energy exists. Ash deposition on the elliptic cylinder bluff body is considered, and its effect on the energy harvesting performance is investigated. Various shapes of ash depositions might lead to different aerodynamic characteristics of the bluff body. Therefore, two bluff bodies with differently shaped ash depositions are designed. **Fig. 2** exhibits the schematic diagram of the two FIVPEHs with different ash deposition attached to the bluff bodies. According to the geometric profile, the bluff bodies presented in **Fig. 2** (a) and (b) are referred to as bell-shaped and horn-like bluff bodies, respectively. According to the literature [44, 45], for a number tubes placed in series in the heat exchange system, the bell-shaped ash deposition is formed only on the first tube. Due to the influence of the wake of the upstream tube, horn-shaped ash depositions are formed on the remaining tubes. Both shapes of ash deposition are present in practice. In order to achieve a FIVPEH with a bell-shaped bluff body, one can install the FIVPEH in the front of all the tubes in the heat exchange system. To obtain a FIVPEH with a horn-shaped bluff body, one can install the FIVPEH at least after the first tube.

Each FIVPEH consists of a bluff body, a cantilever beam, and a piezoelectric transducer. The height of the bluff body is H. The length, width, and thickness of the cantilever beam are L, W, and T_b, respectively. **Fig. 2** (c) shows the key parameters that determine the geometric profiles of the bell-shaped and horn-like bluff bodies. Each bluff body is composed of a principal elliptic cylinder and one/two segmented ellipses. The segmented ellipse is an imitation of the ash deposition. The major and minor axes of the principal ellipse are a_1 and b_1, and $a_1 \times b_1$ = 30 mm × 20 mm. The major and minor axes of the segmented ellipse are a_2 and b_2, and $a_2 \times b_2$ = 24 mm × 10 mm. For the bell-shaped bluff body, the major axes of the principal ellipse and the segmented ellipse are on the same horizontal line. The distance between the left ends of the two ellipses is d_1. Considering that ash deposition may gradually grow, four bell-shaped bluff bodies with different ash deposition sizes are investigated by increasing d_1 from 3 mm to 12 mm with a step of 3 mm. For the horn-like bluff body, the two segmented ellipses are installed symmetrically on the two sides of the major axis of the principal ellipse. The angle between the major axes a_1 and a_2 is 45°. The distance from the end of the segmented ellipse to the edge of the principal ellipse is d_2. Similarly, four different d_2 (3 mm, 6 mm, 9 mm, and 12 mm) are selected to simulate the ash deposition growth.

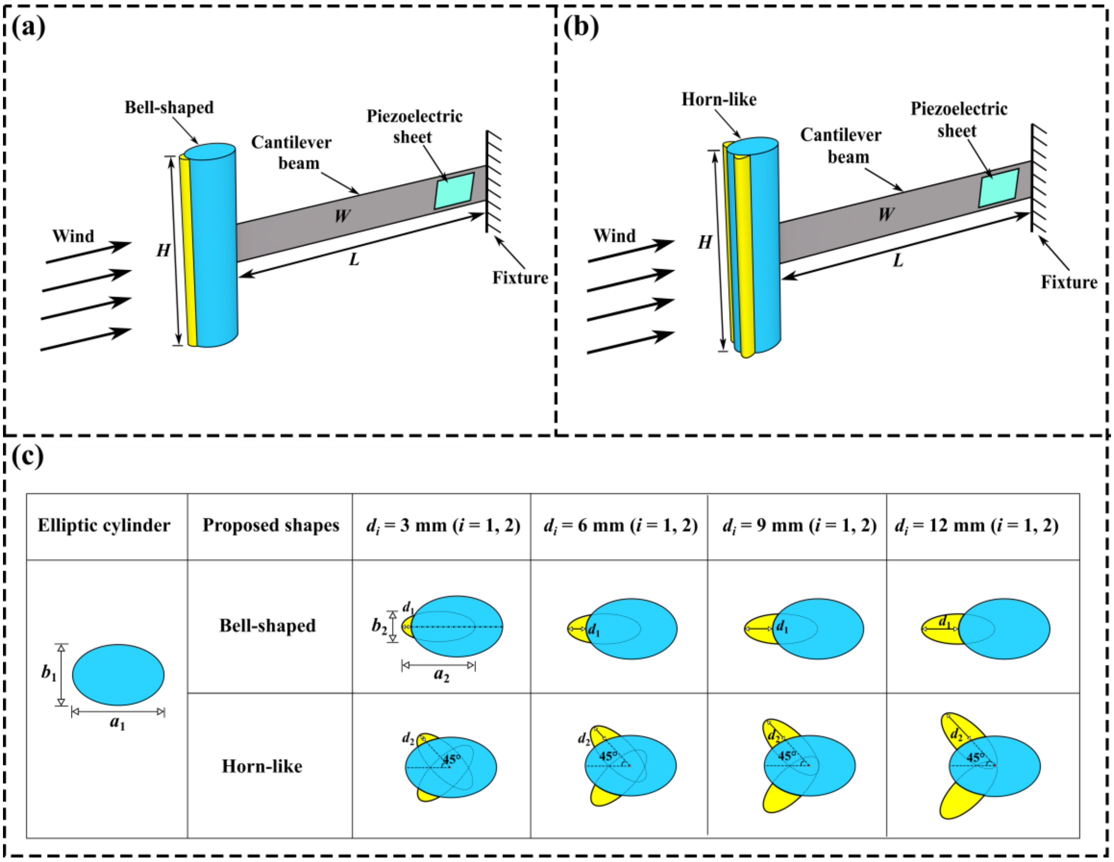

Fig. 2. Schematics of PEHs with different ash depositions: (a) bell-shaped ash deposition; (b) horn-like ash deposition; (c) geometries of the ash deposited bluff bodies.

2.2 Experimental setup

Fig. 3 presents the experimental setup and the physical prototypes of the PEH with bell-shaped and horn-like bluff bodies. A PEH with an ordinary bluff body without ash deposition is used as the baseline model for comparison. In the experiment, the PEHs are, separately, placed in an open wind tunnel with a diameter of 400 mm. The turbulence intensity is controlled to be less than 1.0 %. The bluff body is made of rigid foam material. The major axis, the minor axis, and the height of the elliptic cylinder bluff body are 30 mm, 20 mm, and 118 mm, respectively. The cantilever beam is made of aluminum, and its dimensions are $L \times W \times T_b$ = 184 mm × 25 mm × 0.5 mm. The capacitance C_p of the piezoelectric transducer (PZT-5, Jiaye-shi Co, China) is 24.87 nF. The wind speed in the wind tunnel is controlled by a draught fan and is measured by a hot-wire anemometer (405i, Testo Company, USA). The two-stage honeycomb device straightens the wind generated by the draught fan. The wind speed range investigated in this paper is from 0.87 m/s to 3.61 m/s. The natural frequencies of all the PEHs are calibrated to be almost the same, approximately 8.0 Hz. The displacements of the bluff bodies are measured by a laser displacement sensor (Panasonic: HG-C1400) with a resolution of 300 μm. The signals are recorded using a dual-channel USB data acquisition instrument (USB DAQ-280G). The voltage generated by the piezoelectric transducer is recorded by a data acquisition apparatus (DS1104S, RIGOL, China).

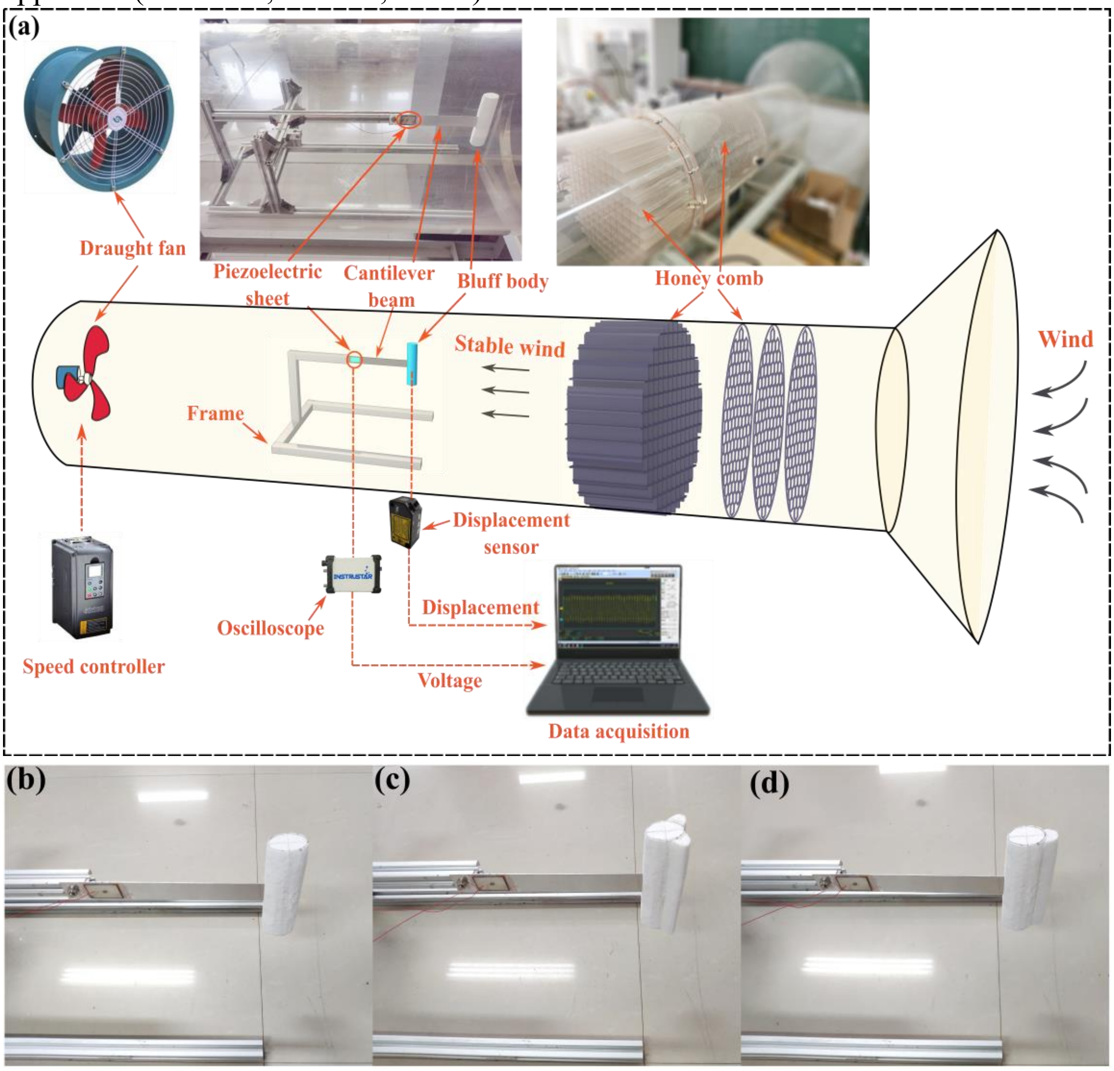

Fig. 3. (a) The experimental setup; (b) the fabricated baseline PEH; (c) the fabricated PEH with the horn-like bluff body; (d) the fabricated PEH with the bell-shaped bluff body.

3. Results and discussion

3.1 The elliptic cylinder bluff body

The wind tunnel test results of the PEH with the elliptic cylinder bluff body are illustrated in **Fig. 4** and **Fig. 5**. **Fig. 4** (a) and (b) present the output voltage and vibration amplitude responses, respectively. A lock-in region, with lower and upper bounds of 1.41 m/s and 2.51 m/s, is observed in the response diagram. It indicates that the PEH with the elliptic cylinder bluff body exhibits VIV. Over the lock-in region, with the increase of wind speed, the output voltage from the PEH first increases, then decreases. A maximum voltage of 2.33 V is obtained when the wind speed reaches 1.82 m/s. When the wind speed exceeds 2.51 m/s beyond the lock-in region, the voltage output becomes negligibly small. The displacement response of the PEH presented in **Fig. 4** (b) exhibits a similar behavior. Appreciable vibration of the PEH occurs only within the lock-in region. The vibration amplitude reaches a maximum value of 7.06 mm at the wind speed of 2.51 m/s.

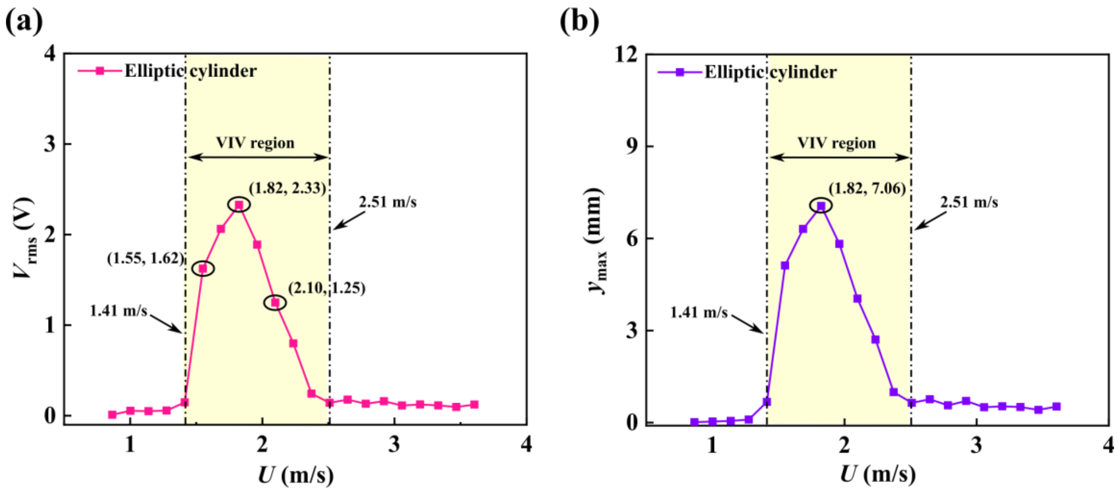

Fig. 4. Results of the PEH with elliptic cylinder bluff body: (a) RMS voltage output (b) maximum vibration displacement of the bluff body.

Fig. 5 exhibits the dominant vibration frequency of the PEH in the VIV region, and the voltage time-history is plotted at the wind speeds of 1.55 m/s, 1.82 m/s, and 2.10 m/s. The three wind speeds are, respectively, taken from the initial excitation branch, upper branch, and lower branch of the VIV region. In **Fig. 5** (a), it is noted that the dimensionless frequency gradually increases to 1 as the wind speed increases, then keeps growing as the wind speed increases. However, the frequency shift in the lock-in region is minor, and the frequency ratio is always around 1. This phenomenon agrees with the results in the literature [47]. Thus, it further proves that the PEH with the elliptic cylinder bluff body performs VIV. It can be seen from **Fig. 5** (b) that at all the three wind speeds, the PEH undergoes harmonic vibration. Due to the locking phenomenon, the output voltage of the PEH at the wind speed of 1.82 m/s is obviously larger than that when the wind speed is changed to 1.55 m/s or 2.10 m/s.

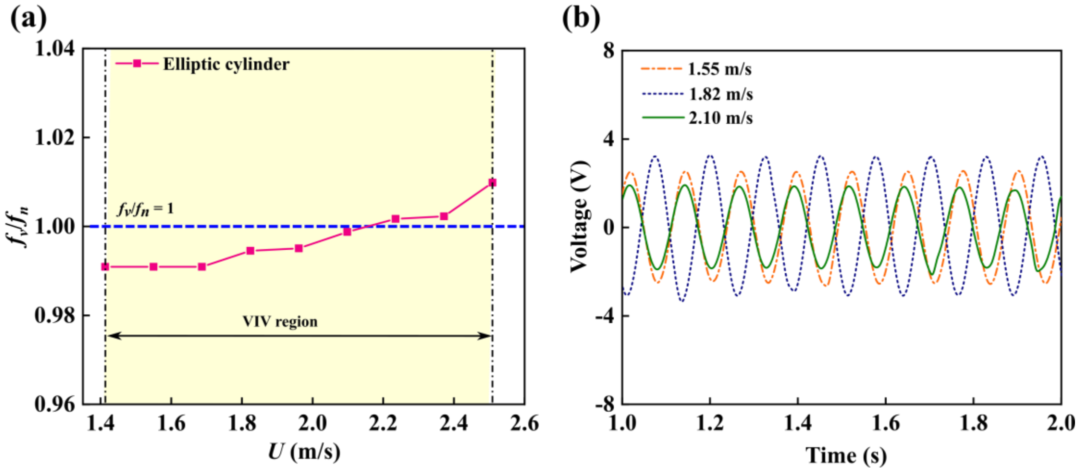

Fig. 5. (a) The dominant non-dimensional frequency of the PEH with elliptic cylinder bluff body under different wind speeds. (b) the voltage output time histories at the wind speeds 1.55 m/s, 1.82 m/s, and 2.10 m/s.

3.2 The Bell-shaped bluff body

As seen in **Fig. 6**, the bell-shaped additions produce a decrease in the amplitude of motion and a reduction of the voltage generated. For the PEH with the elliptic cylinder bluff body, the VIV phenomenon occurs over the wind speed range U = 1.41 m/s ~ 2.51 m/s. A maximum output voltage of 2.33 V is obtained at the wind speed of 1.82 m/s. For the PEH with the bell-shaped bluff body, for d_1 equal to 3 mm, 6 mm, 9 mm, and 12 mm, the maximum voltage correspondingly becomes 0.99 V, 0.77 V, 0.44 V, and 0.49 V, and the maximum amplitude is 3.35 mm, 2.93 mm, 1.75 mm, and 1.79 mm, respectively. In other words, bell-shaped bluff bodies are not beneficial for energy harvesting. In contrast, they demonstrate the potential application for suppressing galloping-induced vibrations. Moreover, optimizing the parameters of the bell-shaped bluff body may lead to a maximum suppression performance. For instance, in the above case studies, the bell-shaped bluff body with d_1 = 9 mm shows the strongest vibration suppression effect: its maximum amplitude is reduced by 75%, compared to the baseline model.

The time history responses of the PEH with the bell-shaped bluff body (d_1 = 9 mm) at U = 1.41 m/s are presented in **Fig. 6** (c) and (d). The results of the baseline model at U = 1.82 m/s are also presented for comparison. U = 1.41 m/s and 1.82 m/s are the optimal wind speeds to achieve the maximum voltage output for each case. Both cases exhibit harmonic vibration, while the baseline model has a significantly larger vibration amplitude, which is consistent with the results in **Fig. 6** (a) and (b).

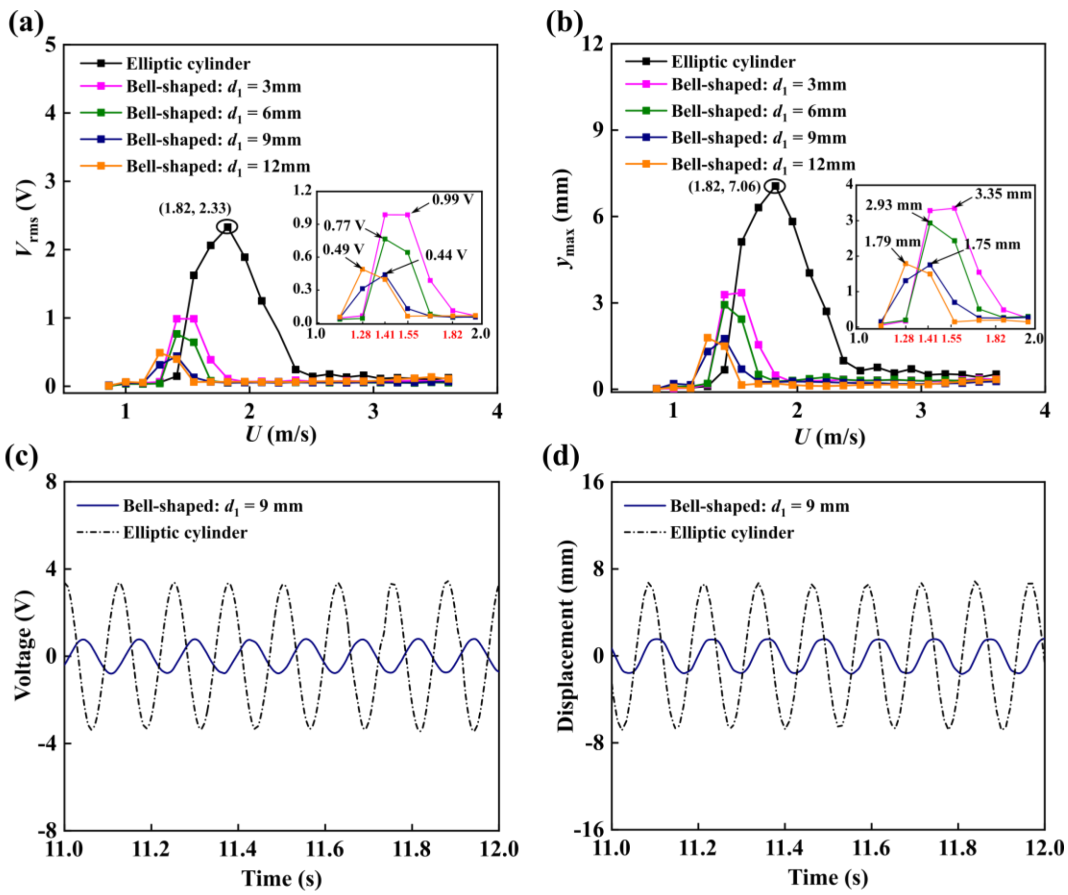

Fig. 6. Performance comparison of the PEHs with different bluff bodies: (a) RMS voltage outputs; (b) maximum vibration displacement of the bluff bodies; (c) time-history voltage output and (d) displacement of the PEHs with the bell-shaped bluff body under the optimal wind speed of U = 1.41 m/s and the elliptic cylinder bluff body under the optimal wind speed of U = 1.82 m/s.

3.3 The Horn-like bluff body

The results of the PEH with the horn-like bluff body of varying d_2 are presented in **Fig. 7**. The results of the baseline model are also provided for comparison. **Fig. 7** (a) clearly shows that, unlike the baseline model, the PEH with the horn-like bluff body mainly exhibits the galloping phenomenon, regardless of the values of d_2. Hence, the PEH with the horn-like bluff body can produce significant voltage outputs over a much wider wind speed range. Moreover, unlike the behavior in the VIV region of the baseline model, with the increase of the wind speed, the voltage output monotonically increases. Over the wind speed range under investigation, for d_2 equal to 3 mm, 6 mm, 9 mm, and 12 mm, the maximum voltage output of the PEH with the horn-like bluff body correspondingly becomes 14.06 V, 14.36 V, 14.20 V, and 14.24 V, which are much larger than that of the baseline model (2.33 V). **Fig. 7** (b) compares the displacement response of the PEH with the horn-like bluff body. For d_2 equal to 3 mm, 6 mm, 9 mm, and 12 mm, the maximum displacement of the PEH with the horn-like bluff body becomes 49.96 mm, 56.32 mm, 54.45 mm, and 55.46 mm, which indicate 607%, 697%, 671%, and 685% increases compared to the baseline model. Among the above cases, using the horn-like bluff body with d_2 of 6 mm leads to the best performance. Its maximum voltage output is increased by 516% compared to the baseline model. In addition, the cut-in wind speed of the optimal design, i.e., d_2 = 6 mm, is about 1.28 m/s, which is smaller by 9% compared to the baseline model. Therefore, using the horn-like bluff body is also favorable for low wind speed energy harvesting.

In fact, the significant increase of the voltage output is the consequence of the galloping phenomenon. And the low cut-in wind speed advantage is inherited from the VIV behavior. In the enlarged views in **Fig. 7** (a) and (b), it is noted that over the wind range 1.1 m/s ~ 1.8 m/s, when d_2 = 3 mm or 6 mm, the PEH with the horn-like bluff body undergoes VIV: the voltage/displacement response first increases, then decreases. When d_2 = 9 mm or 12 mm, the VIV phenomenon appears in the wind speed range of 1.28 m/s ~ 1.69 m/s. The time-history responses of the optimal design (d_2 = 6 mm) at U = 1.82 m/s, which is the optimal wind speed of the baseline model, are presented in **Fig. 7** (c) and (d). It can be seen in **Fig. 7** (a) that both cases exhibit harmonic vibration. Even U = 1.82 m/s is the optimal wind speed of the baseline model, while not for the PEH with the horn-like bluff body; the voltage and displacement responses of the PEH with the horn-like bluff body are still larger than those of the baseline model. In brief, the PEH with the horn-like bluff body demonstrates a superior wind energy harvesting ability.

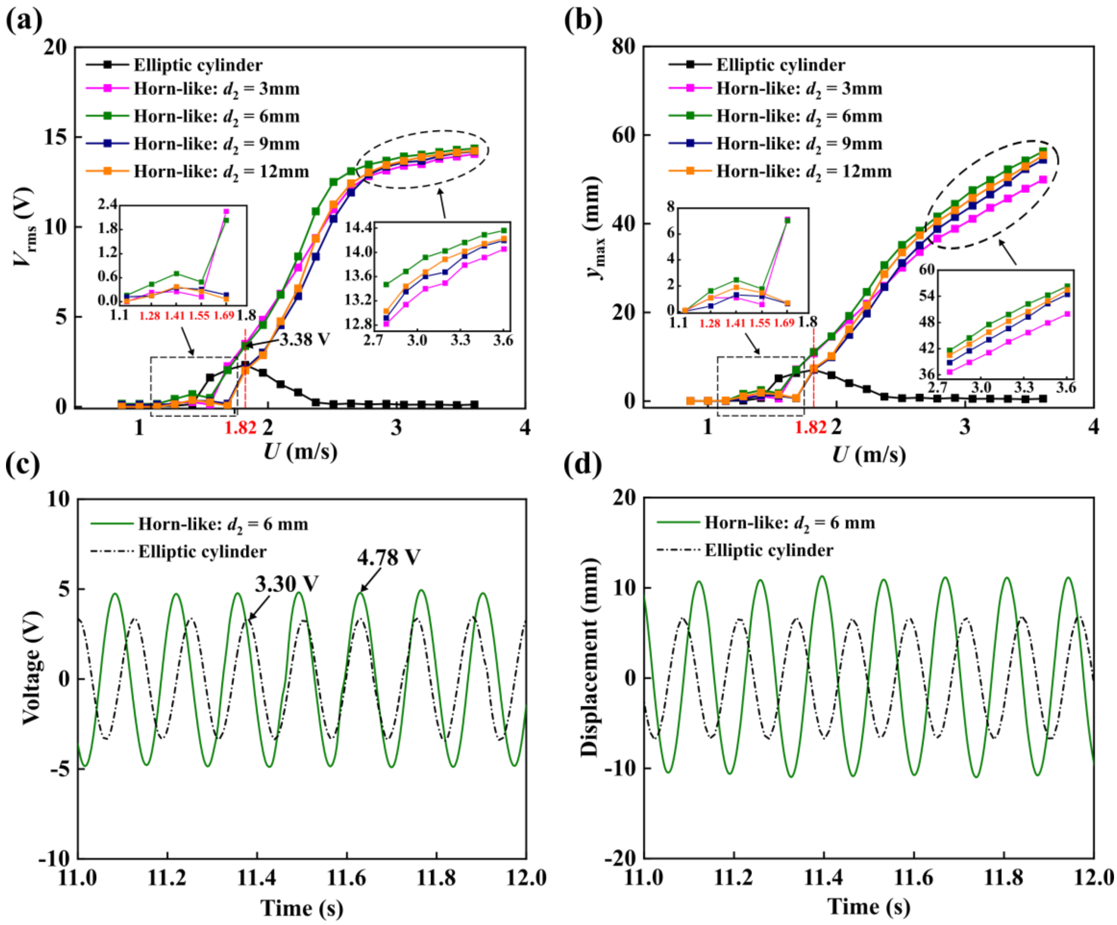

Fig. 7. Performance comparison of the PEHs with different bluff bodies: (a) RMS voltage outputs;

(b) maximum vibration displacement of the bluff bodies; (c) time-history voltage output and (d) displacement of the PEHs with the horn-like bluff body and the elliptic cylinder bluff body under the wind speed of U = 1.82 m/s.

4. Interpretation based on CFD simulation

Computational fluid dynamics (CFD) simulations are carried out to further reveal the effect of ash deposition on the aerodynamics of the bluff body. CFD models are built using the commercial software XFlow, which adopts the lattice Boltzmann method. The dimensions of the bluff bodies in simulations are consistent with those of the physical prototypes tested in the experiments. The calculation domain set in the simulation is a rectangle with a length of $40b_1$ and a width of $20b_1$, where b_1 is the length of the minor axis of the principal ellipse of the bluff body. The left and right boundary conditions of the calculation domain are set as velocity inlet and flow outlet, respectively. The fluid is air. The upper and lower boundary conditions are set to be walls. The distance between the center of the bluff body and the upper boundary is $10b_1$, and that to the outlet boundary is $30b_1$ to ensure that the flow field behind the bluff body can be fully developed. In the CFD simulations, the external single-phase forced incompressible model is selected to simulate the flow. The time step is automatically fixed to 5×10^{-5} s. The Reynolds number of the simulated flow field is approximately 2460.

As known from the results presented in the previous section, using the bell-shaped bluff body leads to vibration suppression and a deteriorated energy harvesting performance. On the contrary, using the horn-like bluff body induces the galloping phenomenon and significantly improves the energy harvesting performance. **Fig. 8** presents the vorticity contours of the bell-shaped (d_1 = 9 mm), elliptic cylinder, and horn-like (d_2 = 6 mm) bluff bodies at different time stages to reveal the aerodynamic mechanisms behind the above conclusion. From **Fig. 8**, one can find that for the bell-shaped bluff body, the presence of a small elliptical bulge in the front streamlines the oncoming flow over the bluff body. Thus, the vortex shedding is similar to that of the elliptic cylinder bluff body: in both cases, primary large-scale vortices (PV) are produced behind the bluff bodies. The width of the wake is evaluated to indicate the intensity of the vortex shedding. The widths of the wake produced after the bell-shaped and elliptic cylinder bluff bodies are $1.57b_1$ and $1.79\ b_1$, respectively. This implies that the intensity of the vortex shedding of the bell-shaped bluff body is weaker than that of the elliptic cylinder. This explains why the vibration amplitude of the bell-shaped bluff body is smaller than that of the elliptic cylinder one. Unlike the elliptic cylinder bluff body, for the horn-like one, due to the presence of two small elliptical bulges, not only primary large-scale vortices (PV), but also small-scale secondary vortices (SV) are produced in the wake flow. Because of the interaction between PV and SV, the vortex shedding effect is delayed, resulting in a significant increase of the wake vortices. Moreover, it is observed that the wake width of the horn-like bluff body is much wider than that of the elliptic cylinder one, which indicates a stronger aerodynamic instability in the wake. Therefore, unlike the vibration mode of the elliptic cylinder bluff body, the vibration mode of the horn-like bluff body is galloping, which can induce a larger-amplitude vibration and produce a higher voltage output. In summary, the formation of small-scale secondary vortices (SV) plays a key role in the intensity of vibration.

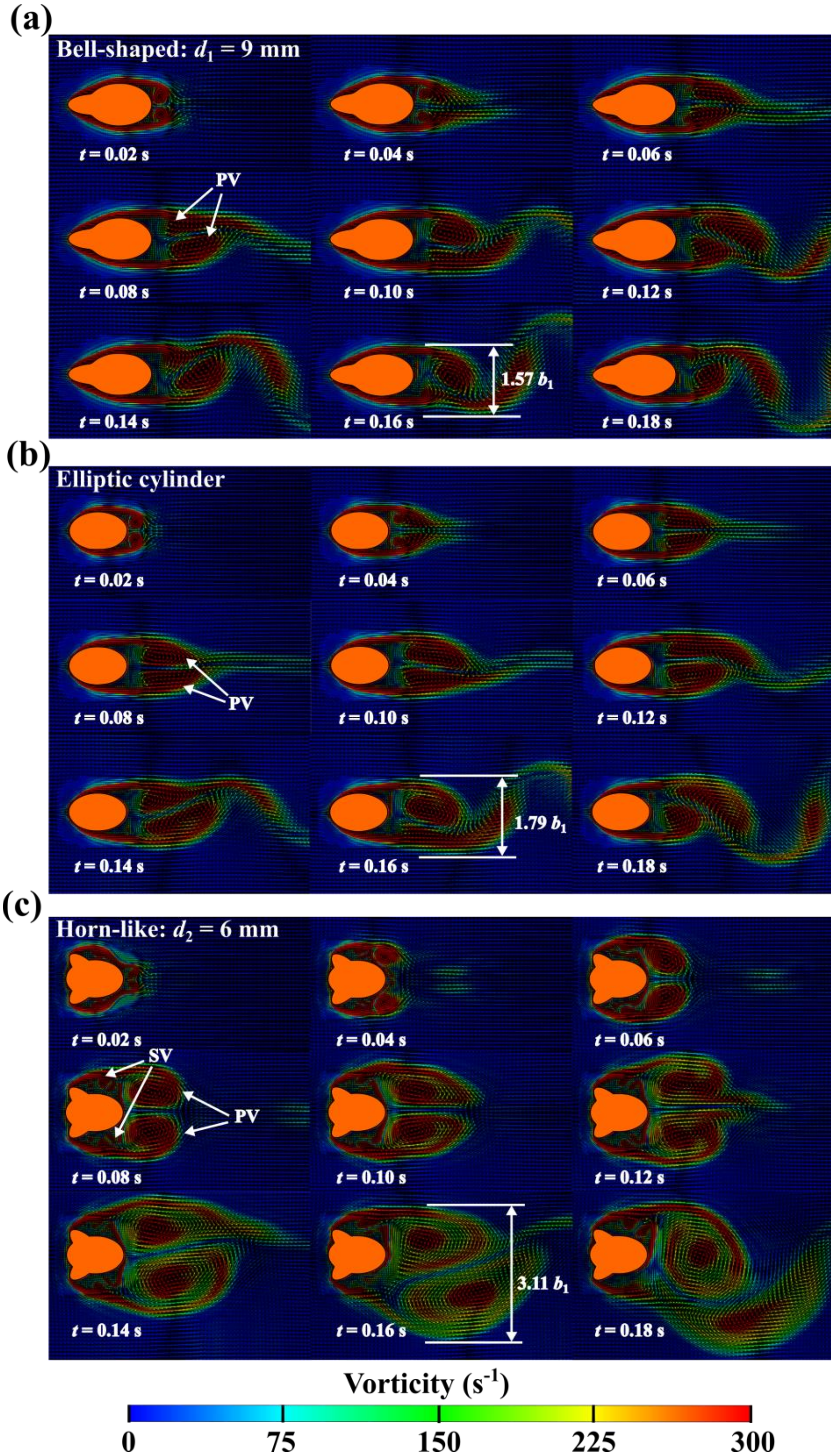

Fig. 8. Comparison of flow-field evolution with time for the three bluff bodies at the wind speed

of U = 1.82 m/s: (a) the bell-shaped (d_1 = 9 mm) bluff body; (b) the elliptic cylinder bluff body; (c) the horn-like (d_2 = 6 mm) bluff body.

The pressure contours around the bell-shaped (d_1 = 9 mm), elliptic cylinder, and horn-like (d_2 = 6 mm) bluff bodies at the wind speed of 1.82 m/s are shown in **Fig. 9**. Obviously, it can be observed that the low-pressure region around the horn-like bluff body is significantly larger than those around the other two bluff bodies. The larger pressure difference causes the horn-like bluff body to vibrate more violently than the other two bluff bodies. Comparing the bell-shaped and elliptic cylinder bluff bodies, the low-pressure region around the bell-shaped bluff body is smaller than that around the elliptic cylinder bluff body. Therefore, the bell-shaped bluff body undergoes the smallest vibration. **Fig. 10** presents the velocity contours of the bell-shaped (d_1 = 9 mm), elliptic cylinder, and horn-like (d_2 = 6 mm) bluff bodies at the wind speed of 1.82 m/s. The high-velocity region in **Fig. 10** corresponds to the low-pressure region in **Fig. 9**. The high-velocity region around the horn-like bluff body is the largest, which enhances the oscillation of the horn-like bluff body, and makes its vibration significantly higher than the other two bluff bodies. The above discussion agrees well with the conclusions obtained from the experiments in the previous section.

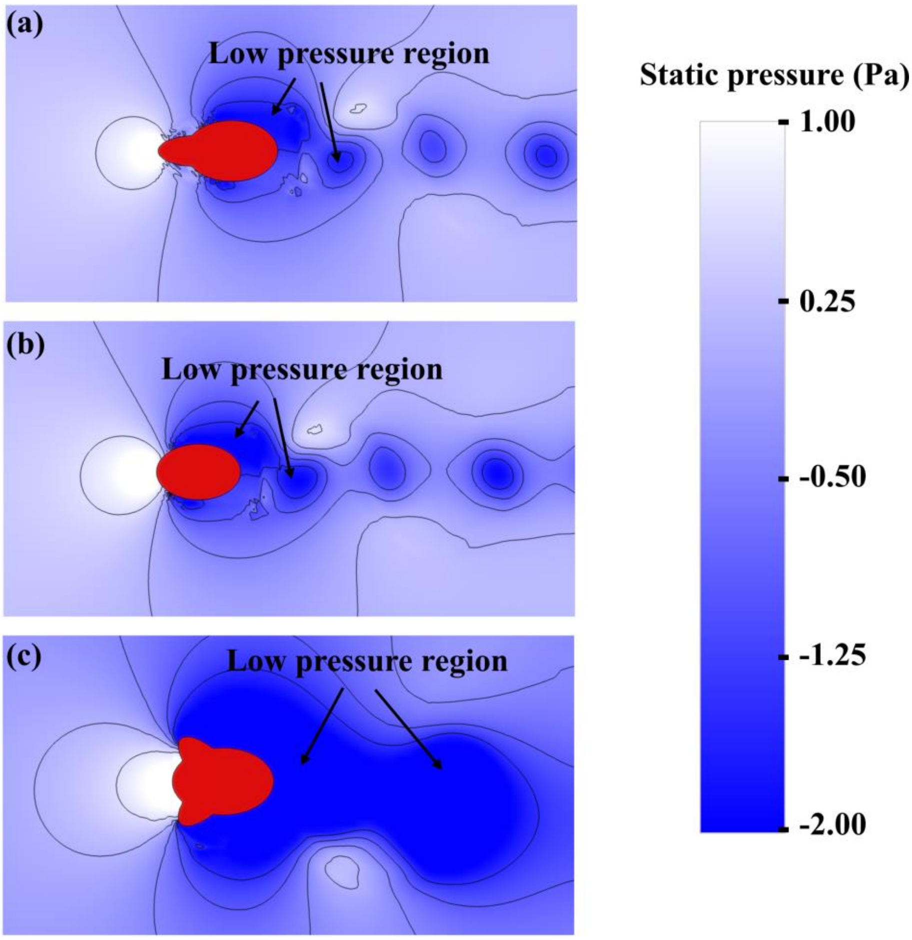

Fig. 9. Pressure contour around (a) the bell-shaped (d_1 = 9 mm) bluff body; (b) the elliptic cylinder bluff body; (c) the horn-like (d_2 = 6 mm) bluff body at the wind speed of 1.82 m/s.

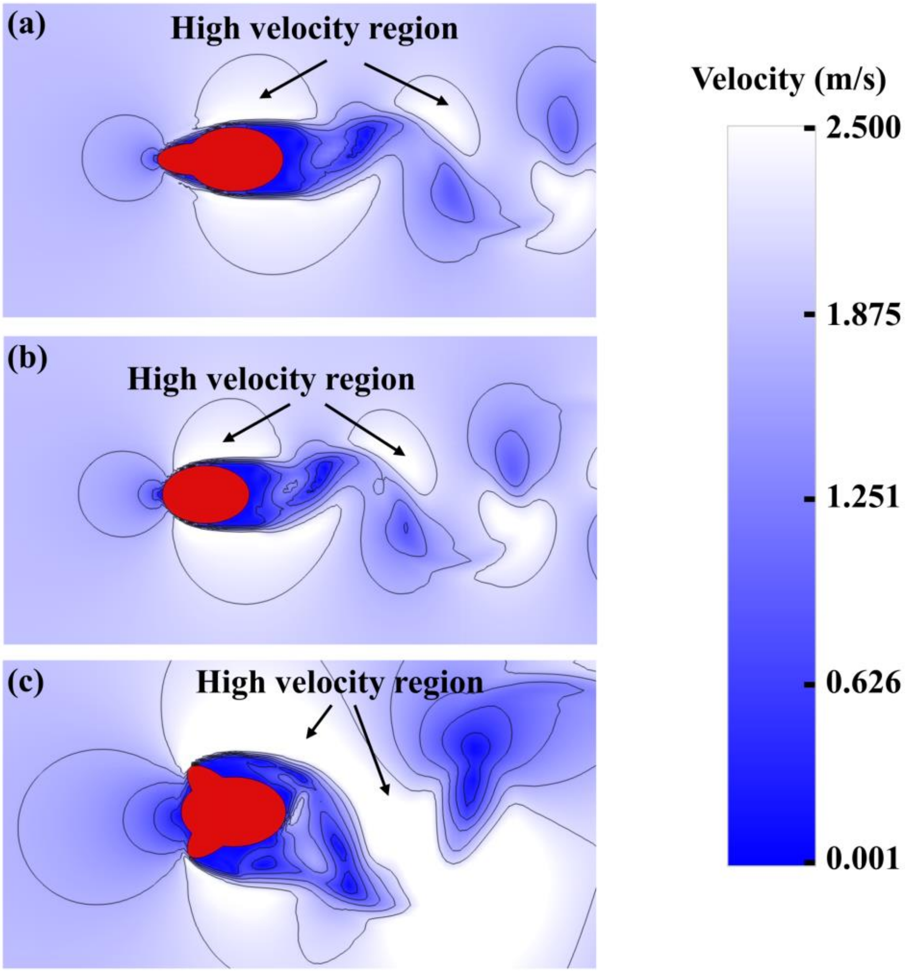

Fig. 10. Velocity contour around (a) the bell-shaped (d_1 = 9 mm) bluff body; (b) the elliptic cylinder bluff body; (c) the horn-like (d_2 = 6 mm) bluff body at the wind speed of 1.82 m/s.

5. Conclusion

This paper has explored the effect of ash deposition on flow-induced vibration energy harvesting in heat exchange systems. According to the shape and size of ash deposition, bell-shaped and horn-like bluff bodies have been proposed to simulate different ash depositions. Experimental results have revealed that the bell-shaped bluff bodies can suppress vibrations and are not beneficial for energy harvesting. In contrast, the horn-like bluff bodies can improve the energy harvesting performance by transforming VIV to galloping. The combination of VIV and galloping reduces the cut-in wind speed of the PEH and increases the voltage outputs under high wind speeds. The voltage output of an optimal prototype with d_2 = 6 mm has been increased by 516%. Besides, CFD simulations have been conducted to interpret the underlying mechanisms behind the phenomena. For the bell-shaped bluff body, a weaker aerodynamic force is generated because the wake width is smaller than that of the elliptic cylinder bluff body. Thus, the vibration of the bluff body is diminished. For the horn-like bluff body, due to the interaction of PV and SV, the wake width is increased, resulting in an increased aerodynamic force. The flow-induced vibration transforms from VIV to galloping. Therefore, a larger voltage output is generated by the PEH with the horn-like bluff body. In summary, a potential usefulness of the harmful ash deposition phenomenon in the flue gas pipeline for benefiting energy harvesting has been proposed and explored. Different ash deposition effects have been investigated. The work presented in this paper represents a preliminary study of the ash deposition effect on flow-induced vibration energy harvesting.

Acknowledgments

This work was supported by the National Natural Science Foundation of China (Grant No. 51977196), the China Postdoctoral Science Foundation (Grant No. 2020T130557), the Natural Science Foundation of Excellent Youth of Henan Province (Grant No. 222300420076), and the State Key Laboratory of Structural Analysis for Industrial Equipment, Dalian University of Technology, China (GZ21114).

References

[1] J. Wang, L. Geng, L. Ding, H. Zhu, D. Yurchenko, The state-of-the-art review on energy harvesting from flow-induced vibrations, Appl. Energy, 267 (2020) 114902.

[2] X.W. Fu, Y.S. Yang, Modeling and analysis of cascading node-link failures in multi-sink wireless sensor networks, Reliab. Eng. Syst. Saf., 197 (2020) 15.

[3] Z. Lai, S. Wang, L. Zhu, G. Zhang, J. Wang, K. Yang, D. Yurchenko, A hybrid piezo-dielectric wind energy harvester for high-performance vortex-induced vibration energy harvesting, Mech. Syst. Signal. Process., 150 (2021).

[4] C. Magazzino, M. Mele, N. Schneider, A machine learning approach on the relationship among solar and wind energy production, coal consumption, GDP, and CO2 emissions, Renew. Energ., 167 (2021) 99-115.

[5] J.J. Yoo, G. Seo, M.R. Chua, T.G. Park, Y.L. Lu, F. Rotermund, Y.K. Kim, C.S. Moon, N.J. Jeon, J.P. Correa-Baena, V. Bulovic, S.S. Shin, M.G. Bawendi, J. Seo, Efficient perovskite solar cells via improved carrier management, Nature, 590 (2021) 10.

[6] C.H. Li, S.C. Xu, J. Yu, Z. Li, W.F. Li, J.H. Wang, A.H. Liu, B.Y. Man, S.K. Yang, C. Zhang, Local hot charge density regulation: Vibration-free pyroelectric nanogenerator for effectively enhancing catalysis and in-situ surface enhanced Raman scattering monitoring, Nano Energy, 81 (2021) 10.

[7] J.L. Wang, S.H. Gu, C.Y. Zhang, G.B. Hu, G. Chen, K. Yang, H. Li, Y.Y. Lai, G. Litak, D. Yurchenko, Hybrid wind energy scavenging by coupling vortex-induced vibrations and galloping, Energy Convers. Manag., 213 (2020) 11.

[8] T. Morbiato, C. Borri, R. Vitaliani, Wind energy harvesting from transport systems: A resource estimation assessment, Appl. Energy, 133 (2014) 152-168.

[9] M.A. Mustapa, O.B. Yaakob, Y.M. Ahmed, C.K. Rheem, K.K. Koh, F.A. Adnan, Wave energy device and breakwater integration: A review, Renew. Sust. Energ. Rev., 77 (2017) 43-58.

[10] C. Chen, Z.Y. Liu, S.H. Wan, J.T. Luan, Q.Q. Pei, Traffic Flow Prediction Based on Deep Learning in Internet of Vehicles, IEEE Trans. Intell. Transp. Syst., 22 (2021) 3776-3789.

[11] H.S. Kim, J.-H. Kim, J. Kim, A review of piezoelectric energy harvesting based on vibration, International Journal of Precision Engineering and Manufacturing, 12 (2011) 1129-1141.

[12] F.K. Shaikh, S. Zeadally, Energy harvesting in wireless sensor networks: A comprehensive review, Renew. Sust. Energ. Rev., 55 (2016) 1041-1054.

[13] S. Fang, X. Fu, X. Du, W.-H. Liao, A music-box-like extended rotational plucking energy harvester with multiple piezoelectric cantilevers, Applied Physics Letters, 114 (2019).

[14] X. Zhao, J. Cai, Y. Guo, C. Li, J. Wang, H. Zheng, Modeling and experimental investigation of an AA-sized electromagnetic generator for harvesting energy from human motion, Smart. Mater. Struct., 27 (2018).

[15] K. Fan, Y. Zhang, S. E, L. Tang, H. Qu, A string-driven rotor for efficient energy harvesting from ultra-low frequency excitations, Appl. Phys. Lett., 115 (2019).

[16] Z. Yang, L. Tang, L. Yu, K. Tao, K. Aw, Modelling and analysis of an out-of-plane electret-based vibration energy harvester with AC and DC circuits, Mech. Syst. Signal. Process., 140 (2020).

[17] G. Hu, C. Zhao, Y. Yang, X. Li, J. Liang, Triboelectric energy harvesting using an origami-inspired structure, Appl. Energy, 306 (2022) 118037.

[18] J. Wang, S. Zhou, Z. Zhang, D. Yurchenko, High-performance piezoelectric wind energy harvester with Y-shaped attachments, Energy Conversion and Management, 181 (2019) 645-652.

[19] A. Abdelkefi, Aeroelastic energy harvesting: A review, International Journal of Engineering Science, 100 (2016) 112-135.

[20] L.B. Zhang, H.L. Dai, A. Abdelkefi, L. Wang, Improving the performance of aeroelastic energy harvesters by an interference cylinder, Appl. Phys. Lett., 111 (2017).

[21] K. Yang, T. Qiu, J. Wang, L. Tang, Magnet-induced monostable nonlinearity for improving the VIV-galloping-coupled wind energy harvesting using combined cross-sectioned bluff body, Smart Materials and Structures, 29 (2020).

[22] K. Yang, J.L. Wang, D. Yurchenko, A double-beam piezo-magneto-elastic wind energy harvester for improving the galloping-based energy harvesting, Appl. Phys. Lett., 115 (2019) 5.

[23] A. Abdelkefi, A.H. Nayfeh, M.R. Hajj, Modeling and analysis of piezoaeroelastic energy harvesters, Nonlinear Dyn., 67 (2011) 925-939.

[24] M. Bryant, E. Garcia, Modeling and Testing of a Novel Aeroelastic Flutter Energy Harvester, Journal of Vibration and Acoustics-Transactions of the Asme, 133 (2011) 011010.

[25] H. Wang, W. Yang, K.D. Nguyen, G. Yu, Wake-induced vibrations of an elastically mounted cylinder located downstream of a stationary larger cylinder at low Reynolds numbers, Journal of Fluids and Structures, 50 (2014) 479-496.

[26] H.D. Akaydin, N. Elvin, Y. Andreopoulos, The performance of a self-excited fluidic energy harvester, Smart. Mater. Struct., 21 (2012).

[27] H.L. Dai, A. Abdelkefi, L. Wang, Theoretical modeling and nonlinear analysis of piezoelectric energy harvesting from vortex-induced vibrations, J. Intell. Mater. Syst. Struct., 25 (2014) 1861-1874.

[28] V. Azadeh-Ranjbar, N. Elvin, Y. Andreopoulos, Vortex-induced vibration of finite-length circular cylinders with spanwise free-ends: Broadening the lock-in envelope, Physics of Fluids, 30 (2018).

[29] G. Hu, K.T. Tse, M. Wei, R. Naseer, A. Abdelkefi, K.C.S. Kwok, Experimental investigation on the efficiency of circular cylinder-based wind energy harvester with different rod-shaped attachments, Appl. Energy, 226 (2018) 682-689.

[30] J.L. Wang, S.K. Sun, L.H. Tang, G.B. Hu, J.R. Liang, On the use of metasurface for Vortex-Induced vibration suppression or energy harvesting, Energy Convers. Manag., 235 (2021) 14.

[31] J.P.D. Hartog, Transmission line vibration due to sleet, Transactions of the American Institute of Electrical Engineers, 51 (1932) 1074-1076.

[32] C. Scruton, Wind effects on structures, James Clayton Lecture, Proceedings Institution of Mechanical Engineers, 185 (1971) 301-317.
[33] G.V. Parkinson, Wind-induced instability of structures, Philosophical Transactions of the Royal Society of London, A269 (1971) 395-409.
[34] G.V. Parkinson, Phenomena and modelling of flow-induced vibrations of bluff bodies, Progress in Aerospace Sciences, 26 (1989) 169-224.
[35] R.D. Blevins, Flow-Induced Vibration, Van Nostrand Reinhold, New York, 1990.
[36] M.P. Païdoussis, S.J. Price, E. De Langre, Fluid-structure interactions: cross-flow-induced instabilities, Cambridge University Press, 2010.
[37] A. Barrero-Gil, G. Alonso, A. Sanz-Andres, Energy harvesting from transverse galloping, J. Sound Vibr., 329 (2010) 2873-2883.
[38] J. Sirohi, R. Mahadik, Harvesting Wind Energy Using a Galloping Piezoelectric Beam, Journal of Vibration and Acoustics-Transactions of the Asme, 134 (2012).
[39] A. Abdelkefi, M.R. Hajj, A.H. Nayfeh, Power harvesting from transverse galloping of square cylinder, Nonlinear Dynamics, 70 (2012) 1355-1363.
[40] J. Wang, S. Sun, G. Hu, Y. Yang, L. Tang, P. Li, G. Zhang, Exploring the potential benefits of using metasurface for galloping energy harvesting, Energy Convers. Manag., 243 (2021).
[41] H. Han, Y.-L. He, W.-Q. Tao, Y.-S. Li, A parameter study of tube bundle heat exchangers for fouling rate reduction, International Journal of Heat and Mass Transfer, 72 (2014) 210-221.
[42] D. Bouris, E. Konstantinidis, S. Balabani, D. Castiglia, G. Bergeles, Design of a novel, intensified heat exchanger for reduced fouling rates, International Journal of Heat and Mass Transfer, 48 (2005) 3817-3832.
[43] S.G. Mavridou, D.G. Bouris, Numerical evaluation of a heat exchanger with inline tubes of different size for reduced fouling rates, International Journal of Heat and Mass Transfer, 55 (2012) 5185-5195.
[44] S.-Z. Tang, Y.-L. He, F.-L. Wang, Y.-B. Tao, Parametric study on fouling mechanism and heat transfer characteristics of tube bundle heat exchangers for reducing fouling considering the deposition and removal mechanisms, Fuel, 211 (2018) 301-311.
[45] Y. Cai, K. Tay, Z. Zheng, W. Yang, H. Wang, G. Zeng, Z. Li, S. Keng Boon, P. Subbaiah, Modeling of ash formation and deposition processes in coal and biomass fired boilers: A comprehensive review, Appl. Energy, 230 (2018) 1447-1544.
[46] S.-Z. Tang, M.-J. Li, F.-L. Wang, Z.-B. Liu, Fouling and thermal-hydraulic characteristics of aligned elliptical tube and honeycomb circular tube in flue gas heat exchangers, Fuel, 251 (2019) 316-327.
[47] Navrose, S. Mittal, Lock-in in vortex-induced vibration, Journal of Fluid Mechanics, 794 (2016) 565-594.

Declaration of Interest Statement (Please upload in word format)

Declaration of interests

☒The authors declare that they have no known competing financial interests or personal relationships that could have appeared to influence the work reported in this paper.

☐The authors declare the following financial interests/personal relationships which may be considered as potential competing interests: